

Semiclassical theory of molecular nonlinear optical polarization

Miguel Angel Sepúlveda^{a)} and Shaul Mukamel

Department of Chemistry, University of Rochester, Rochester, New York 14627

(Received 27 February 1995; accepted 13 March 1995)

The calculation of linear and nonlinear optical response as well as nonadiabatic curve crossing processes depends on the time evolution of the electronic coherences (off-diagonal elements of the density matrix). Unlike their diagonal counterparts, the off-diagonal elements do not have an obvious classical limit. A semiclassical approximation for the nonlinear optical response function, which reveals the classical orbit structure underlying the electronic coherences between Born–Oppenheimer surfaces, is developed. The resulting numerical propagation, which applies to arbitrary anharmonic potentials, is based on integrating the time-dependent Schrödinger equation using the semiclassical time evolution operator, Van Vleck propagator. Using the present formalism it is possible to describe semiclassically multiphoton processes involving several Born–Oppenheimer surfaces. © 1995 American Institute of Physics.

I. INTRODUCTION

Nonlinear optical spectroscopy is a rapidly developing field that has allowed the study of properties of molecular systems in ways that are not possible using linear techniques.^{1–3} Using carefully timed and tuned sequences of ultrashort laser pulses, one can study the evolution of a system in microscopic molecular time scales. Photon echo and hole burning techniques allow the study of molecular interactions with their environment in the liquid or solid state, by completely eliminating inhomogeneous broadening.^{4,5}

When interactions of a chromophore with the environment are taken into account, the numerical calculation of the time evolution becomes a very hard problem. It cannot be easily computed quantum mechanically, although there has recently been some interesting progress in that direction.⁶ If the nuclear degrees of freedom of the chromophore are approximated as harmonic oscillators there are numerous methods to calculate its time evolution, the nonlinear polarizations and optical susceptibilities. We can basically distinguish two methodologies that attempt to address molecular systems with arbitrary potentials; first are the methods based on the classical simulation of the nonlinear response,⁷ and second those based on the approximate evaluation of Feynman path integrals.⁸ The former methods, useful in the limit of strong dissipation and low resolution spectra, have the strength of handling efficiently large number of degrees of freedom and realistic interaction potentials. The methods based on Feynman path integrals are more rigorous and can handle high resolution and less damped dynamics but have some strong limitations related to numerical convergence of oscillatory integrals and intensive computer requirements. Semiclassical techniques for the treatment of molecular systems offer a middle ground between purely classical molecular dynamics and “exact” Feynman paths.⁹ They use classical orbits as a reference zero order path and supplement it with the appropriate quantum phase that repro-

duces even extremely complicated quantum interference.^{10,11}

The nonlinear response functions, which are necessary for describing the nonlinear signal, are most conveniently calculated by propagating the density matrix in Liouville space.^{4,5} The density matrix has several advantages over the wave function formalism: It is fully time ordered and is, therefore, closely related to experiment. It further allows one to more naturally treat mixed states at finite temperatures, and to eliminate unnecessary bath degrees of freedom.

In this paper we combine the nonlinear response function formalism based on the evolution of the density matrix with semiclassical techniques and develop a new method for calculating the nonlinear polarization. Our method is capable of describing asymptotically the electronic coherences that are greatly important in many spectroscopies, and allows the classical interpretation of the dynamics of molecular systems under nonlinear potentials.

At the center of any semiclassical theory in the time domain is the Van Vleck propagator,^{12,13} this is the asymptotic limit of the quantum propagator in coordinate representation (time Green function), $\langle x | \exp[-iHt/\hbar] | x' \rangle$ as $\hbar \rightarrow 0$. The Van Vleck propagator gives the probability amplitude to go from position x' to x in time t . Asymptotically this transition matrix element can be written as the square root of the classical probability for this event, times a phase given by the classical action accumulated along the orbit. Although this has been known for a long time, its practical implementation has been very limited until recently. The numerical effort involved in finding all classical orbits subject to two value boundary conditions was the main obstacle. In order to avoid this difficulty one can represent the Van Vleck formula using the initial value representations.¹⁴

Finally we note that the present formalism can be applied directly to curve crossing and nonadiabatic transitions. This problem is formally identical to the nonlinear response function where the nonadiabatic coupling plays the role of the electric field. The nonadiabatic (second-order) rate constant is related to the linear response and the fourth-order correction is related to the third-order response.^{15,16}

In Sec. II we introduce the nonlinear optical responses

^{a)}Current address: Institute for Fundamental Chemistry, 34-4 Takano-Nishihiraki-cho, Sakyo-ku, Kyoto 606, Japan.

using the density matrix formalism. The formal semiclassical limit is presented in Sec. III and a numerical implementation based on a two-trajectory approximation is developed in Sec. IV. The theory is used for the calculation of the third order response in Sec. V, and applied to a two-electronic state system in Sec. VI. Finally in Sec. VII, we sketch the most general multitrajectory implementation of the semiclassical response function.

II. LIOUVILLE SPACE PATHWAYS FOR THE DENSITY MATRIX

Consider an ensemble of chromophores at equilibrium. Before the interaction with the field $E(t)$, the state of the system is given by the thermal density matrix $\rho^{(0)}(-\infty)$. The time evolution of the chromophore interacting with the field is given by the Liouville–Von Neuman equation

$$\dot{\rho}(t) = -\frac{i}{\hbar}[H, \rho], \quad (1)$$

where H is the sum of the Hamiltonian of the isolated molecular system H_0 and the dipole field–molecule interaction $-\hat{\mu}E(t)$:

$$H = H_0 - \hat{\mu}E(t). \quad (2)$$

We assume that the interaction is weak enough for a perturbation expansion of the density matrix on the field to be valid, $\rho = \rho^{(0)} + \rho^{(1)} + \rho^{(2)} + \dots$.¹ The equations for the successive terms are then given by

$$\dot{\rho}^{(0)}(t) = -\frac{i}{\hbar}[H_0, \rho^{(0)}] = 0, \quad (3a)$$

$$\dot{\rho}^{(n)}(t) = -\frac{i}{\hbar}[H_0, \rho^{(n)}] + \frac{i}{\hbar}[\hat{\mu}E(t), \rho^{(n-1)}]. \quad (3b)$$

Solving the system of coupled equations, Eqs. (3) allows the determination of the polarization of the chromophore $P(t)$. Direct substitution of the density matrix expansion then leads to the expansion of the polarization induced in the chromophore:

$$P(t) = P^{(0)}(t) + P^{(1)}(t) + P^{(2)}(t) + \dots \quad (4)$$

with

$$P^{(n)}(t) = \text{Tr}[\hat{\mu}\rho^{(n)}(t)]. \quad (5)$$

The polarization density of a uniform distribution of chromophores is simply obtained by multiplying the $P^{(n)}$ by N/V , the molar density of chromophores.

The first term in the expansion [Eq. (3a)] gives the time evolution of the initial density matrix subjected to the unperturbed Hamiltonian. Since the initial density matrix represents the equilibrium state of the system, $\rho^{(0)}$ is time independent. The successive terms [Eq. (3b)] can be solved by iteration using the propagator for the unperturbed system, then

$$\rho^{(n)}(t) = \left(\frac{i}{\hbar}\right)^n \int_{-\infty}^t d\tau_n e^{-iH_0(t-\tau_n)/\hbar} \times [\hat{\mu} \cdot E(\tau_n), \rho^{(n-1)}(\tau_n)] e^{iH_0(t-\tau_n)/\hbar}. \quad (6)$$

We thus obtain

$$\rho^{(0)}(t) = \rho^{(0)}(-\infty), \quad (7a)$$

$$\rho^{(1)}(t) = \left(\frac{i}{\hbar}\right) \int_{-\infty}^t d\tau_1 \bar{\rho}^{(1)}(\tau_1; t) E(\tau_1) + \text{h.c.} \quad (7b)$$

$$\rho^{(2)}(t) = \left(\frac{i}{\hbar}\right)^2 \int_{-\infty}^t d\tau_2 \int_{-\infty}^{\tau_2} d\tau_1 \bar{\rho}_2^{(2)}(\tau_1, \tau_2; t) E(\tau_1) E(\tau_2) + \text{h.c.} - \left(\frac{i}{\hbar}\right)^2 \int_{-\infty}^t d\tau_2 \int_{-\infty}^{\tau_2} d\tau_1 \times \bar{\rho}_1^{(2)}(\tau_1, \tau_2; t) E(\tau_1) E(\tau_2), \quad (7c)$$

$$\rho^{(3)}(t) = \left(\frac{i}{\hbar}\right)^3 \int_{-\infty}^t d\tau_3 \int_{-\infty}^{\tau_3} d\tau_2 \int_{-\infty}^{\tau_2} d\tau_1 \times \bar{\rho}_2^{(3)}(\tau_1, \tau_2, \tau_3; t) E(\tau_1) E(\tau_2) E(\tau_3) + \text{h.c.} + \left(\frac{i}{\hbar}\right)^3 \int_{-\infty}^t d\tau_3 \int_{-\infty}^{\tau_3} d\tau_2 \int_{-\infty}^{\tau_2} d\tau_1 \times \bar{\rho}_1^{(3)}(\tau_1, \tau_2, \tau_3; t) E(\tau_1) E(\tau_2) E(\tau_3) + \text{h.c.} \quad (7d)$$

The symbol h.c. stands for the Hermitian conjugate of the previous expression. In Eqs. (7) we have introduced the Liouville space generating functions for the density matrix of the n th order, $\bar{\rho}_k^{(n)}$, which are defined as follows

$$\bar{\rho}^{(1)}(\tau_1; t) = e^{-iH_0 t/\hbar} \hat{\mu}(\tau_1) \rho^{(0)}(-\infty) e^{iH_0 t/\hbar}, \quad (8a)$$

$$\bar{\rho}_2^{(2)}(\tau_1, \tau_2; t) = e^{-iH_0 t/\hbar} \hat{\mu}(\tau_2) \hat{\mu}(\tau_1) \rho^{(0)}(-\infty) e^{iH_0 t/\hbar}, \quad (8b)$$

$$\bar{\rho}_1^{(2)}(\tau_1, \tau_2; t) = e^{-iH_0 t/\hbar} \hat{\mu}(\tau_1) \rho^{(0)}(-\infty) \hat{\mu}(\tau_2) e^{iH_0 t/\hbar}, \quad (8c)$$

$$\bar{\rho}_2^{(3)}(\tau_1, \tau_2, \tau_3; t) = e^{-iH_0 t/\hbar} \hat{\mu}(\tau_3) \hat{\mu}(\tau_2) \hat{\mu}(\tau_1) \times \rho^{(0)}(-\infty) e^{iH_0 t/\hbar}, \quad (8d)$$

$$\bar{\rho}_1^{(3)}(\tau_1, \tau_2, \tau_3; t) = e^{-iH_0 t/\hbar} \hat{\mu}(\tau_3) \rho^{(0)}(-\infty) \hat{\mu}(\tau_1) \times \hat{\mu}(\tau_2) e^{-iH_0 t/\hbar}. \quad (8e)$$

We have made use of the Heisenberg representation of the transition dipole moment $\hat{\mu}(t)$:

$$\hat{\mu}(t) = e^{iH_0 t/\hbar} \hat{\mu} e^{-iH_0 t/\hbar}. \quad (9)$$

Notice that the second integrals in Eqs. (7c) and (7d) are not time ordered. It is preferable to work with time-ordered expressions that can be easily interpreted in terms of sequences of light pulses. We then recast Eqs. (7c) and (7d) as

$$\rho^{(2)}(t) = \left(\frac{i}{\hbar}\right)^2 \int_{-\infty}^t d\tau_2 \int_{-\infty}^{\tau_2} d\tau_1 \left[\sum_{j=1}^2 \hat{Q}_j(\tau_1, \tau_2; t) + \text{h.c.} \right] \times E(\tau_1) E(\tau_2), \quad (10a)$$

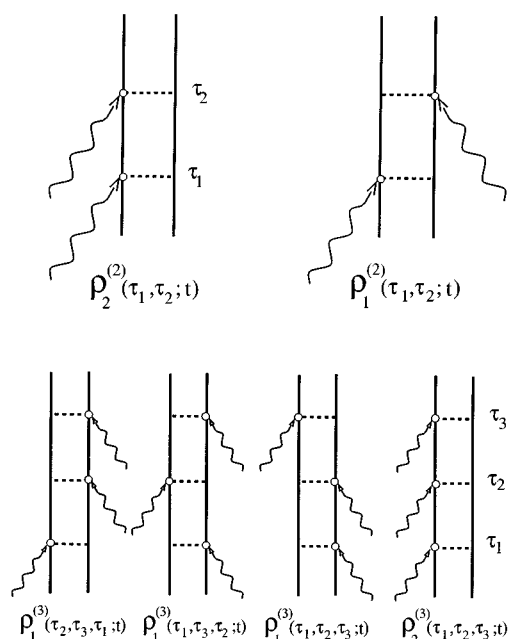


FIG. 1. Double-sided Feynman diagram for the two generating functions contributing to the density matrix term $\rho^{(2)}$ and $\rho^{(3)}$. **Top:** Second-order terms, **Bottom:** Third order terms.

$$\rho^{(3)}(t) = \left(\frac{i}{\hbar}\right)^3 \int_{-\infty}^t d\tau_3 \int_{-\infty}^{\tau_3} d\tau_2 \int_{-\infty}^{\tau_2} d\tau_1 \times \left[\sum_{j=1}^4 \hat{R}_j(\tau_1, \tau_2, \tau_3; t) - \text{h.c.} \right] \times E(\tau_1)E(\tau_2)E(\tau_3). \quad (10b)$$

Now the time variables τ_1, τ_2, τ_3 are ordered, i.e., that $\tau_1 \leq \tau_2 \leq \tau_3$. The time-ordered form is obtained naturally when the Liouville equation for the density matrix is solved. The operators \hat{Q}_j and \hat{R}_j contain the complete information necessary for the calculation of the nonlinear response functions. These operators are defined in terms of the generating functions introduced previously as

$$\hat{Q}_1(\tau_1, \tau_2; t) = -\bar{\rho}_1^{(2)}(\tau_1, \tau_2; t), \quad (11a)$$

$$\hat{Q}_2(\tau_1, \tau_2; t) = \bar{\rho}_2^{(2)}(\tau_1, \tau_2; t), \quad (11b)$$

$$\hat{R}_1(\tau_1, \tau_2, \tau_3; t) = \bar{\rho}_1^{(3)}(\tau_2, \tau_3, \tau_1; t), \quad (12a)$$

$$\hat{R}_2(\tau_1, \tau_2, \tau_3; t) = \bar{\rho}_1^{(3)}(\tau_1, \tau_3, \tau_2; t), \quad (12b)$$

$$\hat{R}_3(\tau_1, \tau_2, \tau_3; t) = \bar{\rho}_1^{(3)}(\tau_1, \tau_2, \tau_3; t), \quad (12c)$$

$$\hat{R}_4(\tau_1, \tau_2, \tau_3; t) = \bar{\rho}_2^{(3)}(\tau_1, \tau_2, \tau_3; t). \quad (12d)$$

Each of these terms constitutes a pathway for the propagation of the density matrix in Liouville space,² and can be represented by a double-sided Feynman diagram (Fig. 1). The generating functions contain all the dynamical information of the system, but a given spectroscopic measurement selects only part of that information.

Two kinds of quantum interference show up in the nonlinear optical response function. The first is due to the bra and ket dynamics itself, several quantum paths contribute to their dynamics and the phase interference between the paths create typical quantum effects. Second, because the total response functions consists of the sum of several bra-ket propagations, or Feynman diagrams, an additional interference pattern is created. Each of the Feynman diagrams, or ways in which light pulses interact with the system at a certain order, have a completely different dynamical time evolution. In the language used in previous paragraphs, several of the generating functions contribute to the same dipole expectation value. For example, the two generating functions, $\bar{\rho}_1^{(2)}$ and $\bar{\rho}_2^{(2)}$ make the second-order term $\rho^{(2)}$ and consequently $P^{(2)}$. Their Feynman diagrams allow one to visualize the two ways in which two laser pulses interact via the density matrix. In the case of $\bar{\rho}_2^{(2)}$ both pulses act on the ket side while in the $\bar{\rho}_1^{(2)}$ one pulse interacts on the ket and at a different time a second pulse acts on the bra side of the density matrix. The sum of both generating functions provides the second kind of interference.

A fully quantum calculation of the generating functions requires a simultaneous propagation of the bra and the ket. In general, it is not easy to calculate the generating functions exactly for realistic systems. However, sometimes the coupling of the chromophore with an external bath makes the system evolve in time classically. Semiclassical approaches for the calculation of these quantities can then be both numerically and physically very useful. Semiclassical equations of motion for these generating functions were developed in Ref. 15. The equations were derived by assuming that the Liouville generating function has a Gaussian form in phase space at all times. The equations describe the evolution in terms of a single reference trajectory which represents both the bra and the ket. The actual density matrix depends on the evolution in the vicinity of that trajectory. This information is carried out by the second moments of the wave packet in phase space. The generating functions may be obtained by running a set of classical trajectories launched in the region covered by the initial density matrix.¹⁷ The path followed by the classical orbits are determined not only by the Hamiltonian of the system H_0 , but by the particular combination of propagators implicit in the different generating functions in Eqs. (8). A basic limitation of this procedure is the need to construct an effective reference Hamiltonian which should reproduce both the bra and the ket evolution. This can be only done rigorously for harmonic systems. The resulting equations of motion are exact, e.g., for a two electronic level system with harmonic potentials that differ in their equilibrium position and frequency. For harmonic models it is also possible to include dissipation by coupling to a harmonic bath.¹⁸ For anharmonic systems there is no general way to construct this reference Hamiltonian and the procedure is, therefore, limited to short times and small anharmonicities. In this paper we develop a new semiclassical Green function propagation scheme that overcomes the limitations of the reference Hamiltonian approach and allows the asymptotic propagation of bra and ket in general anharmonic potentials. The relevant classical orbits come in pairs, one for

TABLE I. Left and right operators for the third-order generating function $\bar{\rho}_i^{(3)}$, $i=1,2$.

$\hat{\mathcal{Q}}_i^L = e^{iH_0 t/\hbar}$
$\hat{\mathcal{Q}}_i^R = e^{-iH_0(t-\tau_3)/\hbar} \hat{\mu} e^{-iH_0(\tau_3-\tau_2)/\hbar} \hat{\mu} e^{-iH_0(\tau_2-\tau_1)/\hbar} \hat{\mu} e^{-iH_0\tau_1/\hbar}$
$\hat{\mathcal{Q}}_i^L = e^{iH_0\tau_1/\hbar} \hat{\mu} e^{iH_0(\tau_2-\tau_1)/\hbar} \hat{\mu} e^{iH_0(t-\tau_2)/\hbar}$
$\hat{\mathcal{Q}}_i^R = e^{-iH_0(t-\tau_3)/\hbar} \hat{\mu} e^{-iH_0\tau_3/\hbar}$

the time evolution of the ket and one for the bra. By retaining the bra and ket time evolutions separately we obtain an improved approximation that better mimics the original quantum problem.

III. SEMICLASSICAL LIMIT OF THE LIOUVILLE SPACE GENERATING FUNCTIONS

All the fundamental spectroscopic observables can be derived from $\rho^{(n)}$, and consequently from the operators \hat{Q}_j 's \hat{R}_j 's. Four-wave mixing spectroscopic measurements directly probe the nonlinear responses R_j 's while the functions Q_j 's are related to three-wave spectroscopies.

In general it is not easy to calculate the generating functions exactly for realistic systems. However sometimes the coupling of the chromophore with an external bath makes the system evolve in time more classically. Semiclassical approaches for the calculation of these quantities can then be both numerically and physically very useful.

The passage to the asymptotic limit $\hbar \rightarrow 0$ is carried out by writing Eqs.(8) in the coordinate representation

$$\langle x_l | \bar{\rho}_i^{(n)} | x_r \rangle = \int dx_r' dx_l' \langle x_l | \hat{\mathcal{Q}}_i^L | x_l' \rangle \times \langle x_l' | \rho^{(0)}(-\infty) | x_r' \rangle \langle x_r' | \hat{\mathcal{Q}}_i^R | x_r \rangle. \quad (13)$$

Both operators to the left and right of the initial $\rho^{(0)} \times(-\infty)$ are the time evolution operator for the initial density matrix that yields the i th generating function to n th order at time t . The formulas for the left and right operators of the third-order term are given in Table I. Left and right operators obviously depend on n , the perturbation order, but we have omitted this index from Eq. (13) for the sake of simplicity.

The basic building block for semiclassics in the time domain is the Van Vleck propagator^{9,12,13}

$$\lim_{\hbar \rightarrow 0} \langle x_l | \exp[-iHt/\hbar] | x_r \rangle \approx (2\pi i\hbar)^{-1/2} \sum \left| \frac{dp'}{dx_r} \right|^{1/2} \exp \left[\frac{i}{\hbar} S(x_l, x_r) - \frac{i\pi}{2} \mu \right]. \quad (14)$$

Equation (14) is the asymptotic limit of the time-dependent Green function. From the correspondence principle we know that the modulus square of this element is the classical probability of going from x' to x_t as $\hbar \rightarrow 0$. The classical probability is given by $|dp'/dx_r|$ (see Appendix A). The phase factor $S(x_r, x')$ is the classical action accumulated along the classical orbit launched at x' and arriving at x_t . This action is easily calculated by integrating the Lagrangian of the system along the classical orbit:

$$S = \int_{x'}^{x_t} \mathcal{L}(\dot{x}_{t'}, x_{t'}) dt'. \quad (15)$$

The sum runs over all possible classical orbits satisfying the given boundary conditions x_t, x' at the specific time t . When there is only one orbit in the sum then the semiclassical transition probability is identical to the classical, as is the case for the harmonic oscillator. However, in general, there will be more than one orbit in the sum, and in that case the probability amplitude will not be simply the sum of classical probability amplitudes but, due to the phases, there will be an interference. Finally the factor μ in the exponent is an integer known as the Morse index (not to be confused with the dipole moment operator $\hat{\mu}$). It was introduced by Gutzwiller to extend the validity of Van Vleck's original formula beyond caustics.¹³ The Morse index is normally calculated by counting the number of times dx_t/dp' goes through zero along the orbit. Using the stability analysis summarized in Appendix A, this is also equivalent to detecting the number of times the stability matrix element M_{21} changes sign along the orbit. The zero's counting procedure is applicable when $(\partial^2 H/\partial p^2) > 0$, which is generally the case. For other kinds of Hamiltonians a different procedure is followed for calculating the Morse index.¹⁹ The semiclassical formula [Eq. (14)] has been used to calculate the linear response of a multidimensional nonlinear system subject to an electromagnetic field.²⁰

Generally the Hamiltonian H_0 will be the sum over several Born–Oppenheimer surfaces corresponding to adiabatic electronic states $|e_i\rangle$:

$$H_0 = \sum_{i=1} |e_i\rangle H_i \langle e_i|. \quad (16)$$

Similarly the dipole moment operator is a sum over the dipole couplings between the different electronic states (for a molecule with no permanent dipole)

$$\hat{\mu} = \sum_{i \neq j} |e_i\rangle \hat{\mu}_{ij} \langle e_j|. \quad (17)$$

Using the above expressions for the Hamiltonian, the dipole moment and the semiclassical Green function we derive formulas for the left–right propagators $\hat{\mathcal{Q}}_i^L$ and $\hat{\mathcal{Q}}_i^R$ as the product of several Van Vleck propagators integrated over the intermediate nuclear coordinates:

$$\langle x_l | \hat{\mathcal{Q}}_i^L | x_l' \rangle = \int dx_1, \dots, dx_k \langle x_l | e^{-iH_{i_1}\tau_1/\hbar} | x_1 \rangle \times \langle x_1 | \hat{\mu}_{i_1, i_2} | x_2 \rangle \dots \langle x_{k-1} | \hat{\mu}_{i_{k-1}, i_k} | x_k \rangle \times \langle x_k | e^{-iH_{i_k}\tau_k/\hbar} | x_l' \rangle, \quad (18a)$$

$$\langle x_r' | \hat{\mathcal{Q}}_i^R | x_r \rangle = \int dx_1, \dots, dx_k \langle x_r' | e^{-iH_{i_1}\tau_1/\hbar} | x_1 \rangle \times \langle x_1 | \hat{\mu}_{i_1, i_2} | x_2 \rangle \dots \langle x_{k-1} | \hat{\mu}_{i_{k-1}, i_k} | x_k \rangle \times \langle x_k | e^{-iH_{i_k}\tau_k/\hbar} | x_r \rangle. \quad (18b)$$

The dipole operator couplings transform the generating functions into a sequential chain of propagators on different electronic surfaces i_1, i_2, \dots

In the Condon approximation, which will be used in this article, the transition dipole moment is assumed to slowly vary with respect to the nuclear degrees of freedom. Then the $\langle x_{k-1} | \hat{\mu}_{i,j} | x_k \rangle$ elements are constant functions with respect to the nuclear degrees of freedom. In this approximation we will set all the $\hat{\mu}_{i,j} = 1$. Integration of Eqs. (18) over the intermediate positions gives essentially the probability amplitude to go from x'_l to x_l when propagating for τ_1 on an electronic state, τ_2 on another electronic state, etc. In the non-Condon approximation the explicit coordinate dependence of the transition dipole moments can still be taken into account by linearly expanding the dipole function about the classical orbit running between initial and final positions.

The integration of Eqs. (18) are still very difficult because it involves the determination of k classical orbits for every x'_l, x_l pair and for every set of times. Moreover momentum is not necessarily preserved when passing from the path $x'_l - x_k$ to $x_k - x_{k-1}$; all the orbits are disjointed in principle (Fig. 2). However, in the asymptotic $\hbar \rightarrow 0$ limit we can calculate the integrals [Eqs. (18a) and (18b)] by stationary phase. Doing so we obtain

$$\langle x_l | \hat{\mathcal{L}}_i^l | x'_l \rangle \approx (2\pi i \hbar)^{-1/2} \left| \frac{\partial^2 S_l}{\partial x_l \partial x'_l} \right|^{1/2} \times \exp \left[\frac{i}{\hbar} S_l(x_l, x'_l) - \frac{i\pi}{2} (\mu_l + \delta_l) \right], \quad (19a)$$

$$\langle x'_r | \hat{\mathcal{L}}_i^r | x_r \rangle \approx (-2\pi i \hbar)^{-1/2} \left| \frac{\partial^2 S_r}{\partial x_r \partial x'_r} \right|^{1/2} \times \exp \left[-\frac{i}{\hbar} S_r(x_r, x'_r) + \frac{i\pi}{2} (\mu_r + \delta_r) \right], \quad (19b)$$

where the actions $S_r(x_r, x'_r)$ and $S_l(x_l, x'_l)$ are calculated along the stationary paths going classically from x'_l to x_l on the left and from x'_r to x_r on the right operators. Both stationary paths are sequences of classical orbits subject to the condition of momentum and position conservation when switching between electronic states. This condition is a direct consequence of the last stationary phase approximation. Then the left stationary path, for example, will start at x'_l , go forward τ_1 in time, switch potential surface staying on the same spot in phase space, and continues for τ_2 , etc. ... until completing the sequence of evolution operators in $\hat{\mathcal{L}}_i^l$. The indices μ_r and μ_l are the sums of the right-left Morse indices along the classical segments in the stationary path (see Fig. 1). There are also additional phase shifts δ_l, δ_r that arise from the stationary phase approximation and are a result of constructing the full semiclassical propagator from several shorter ones. We will deal in more detail with the determination of the δ index later. By convention the paths for the left and right operators run forward in time. Looking back to the expression for the generating functions, Eq. (13), it is straightforward to write down its semiclassical limit by substituting the left-right propagators by Eqs. (19).

Our next concern would be how to evaluate this expression in practice. The simplest possible approach is explained in Sec. IV. It is based on the Gaussian wave packet method^{21,22} and consists of expanding the classical dynamics about a pair of classical orbits. We will then apply this method to a two level chromophore in Sec. VI.

IV. SEMICLASSICAL EXPANSION OF THE GENERATING FUNCTION

Given the semiclassical expressions for the left and right propagators [Eqs. (19)] it would seem that the only step necessary for the determination of the generating functions is the integration of Eq. (13). For four-wave mixing experiments we need to evaluate the third-order generating functions $\bar{\rho}_i^{(3)}$ $i=1,2$, then

$$\langle x_l | \bar{\rho}_i^{(3)} | x_r \rangle \approx \frac{1}{2\pi\hbar} \int dx'_r dx'_l \langle x'_l | \rho^{(0)}(-\infty) | x'_r \rangle | \mathcal{M}_{21}^l \mathcal{M}_{21}^r |^{-1/2} \times \exp \left[\frac{i}{\hbar} S_l(x_l, x'_l) - \frac{i}{\hbar} S_r(x_r, x'_r) - \frac{i\pi}{2} (\Delta\mu + \Delta\delta) \right], \quad (20)$$

where $\Delta\mu = \mu_l - \mu_r$ and $\Delta\delta = \delta_l - \delta_r$.

The integration is carried out over all possible initial position pairs x'_l, x'_r . We have made use of the total stability matrix along the left and right propagations, \mathcal{M}^l and \mathcal{M}^r , as defined in Appendix A. The action functions have a complicated dependence on initial and final positions mainly due to the root search problem mentioned earlier; for every set of initial-final conditions the appropriate initial momenta must be determined in order to obtain the actions and phase shifts. In general the calculation of this integral seems numerically very challenging. Nevertheless, several approximations can be shown to give extraordinarily good results thanks to the localization of the initial state. The function $\langle x'_l | \rho^{(0)}(-\infty) | x'_r \rangle$ in the integrand is often nonzero only in a limited region of configuration space. This reduces the amount of computational effort. Moreover, if the initial state is localized in a relatively small region, one can expand the classical actions and dynamics about the center of the distribution. Let us assume that the initial density matrix is Gaussian:

$$\langle x'_l | \rho^{(0)}(-\infty) | x'_r \rangle = \sqrt{\frac{2(\alpha - \gamma)}{\pi}} \times \exp[-\alpha(x'_l)^2 - \alpha(x'_r)^2 + 2\gamma x'_l x'_r]. \quad (21)$$

For example, for a harmonic oscillation at equilibrium the parameters α and γ are given by

$$\alpha = \frac{m\omega}{2\hbar} \coth(\beta\hbar\omega), \quad (22a)$$

$$\gamma = \frac{m\omega}{2\hbar \sinh(\beta\hbar\omega)}, \quad (22b)$$

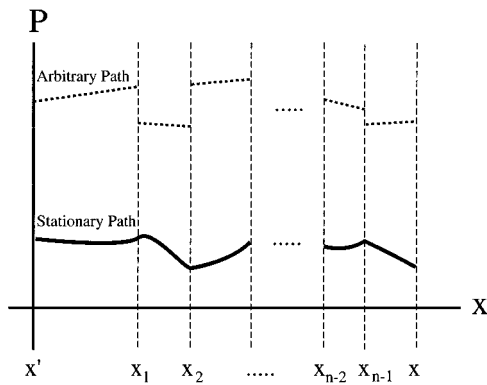


FIG. 2. Phase space diagram of two kinds of paths contributing to the left or right propagators: An arbitrary quantum path for the left (right) propagator between x', x (dash line), and the stationary “point” (solid line) which is simply a classically connected orbit joining x', x .

where $\beta = 1/kT$. If the initial density matrix is not Gaussian, either because the electronic surface is not harmonic or the initial ensemble is not in equilibrium, one can always decompose $\rho^{(0)}(-\infty)$ as a sum over Gaussians localized in configuration space.

The basic approximation for the two-orbit semiclassical expansion is to assume that the dynamics of the bra and the ket can be approximated as a moving Gaussian along the classical orbit launched at the center of the initial density matrix. The center position of the $\rho^{(0)}(-\infty)$ is $x'_i = 0$, $x'_r = 0$ and the average momenta $p'_i = 0$, $p'_r = 0$. From this single point two classical orbits (\bar{x}_l, \bar{x}_r) depart and follow the dynamics specified by the left and right time evolutions. Logically any other classical orbit whose initial conditions were taken in the nearby region of phase space would lead to a different classical path. Nevertheless for a short time it is valid to represent every orbit departing from arbitrary initial positions x'_l, x'_r and momenta p'_l, p'_r and reaching x_l, x_r by expanding around the two orbits that initiate their dynamics at the center of the initial density matrix (see Fig. 3). Upon linearization of the equations of motion along the guiding orbits we write

$$p_l \approx \bar{p}_l + \mathcal{M}_{11}^l p'_l + \mathcal{M}_{12}^l x'_l, \quad (23a)$$

$$x_l \approx \bar{x}_l + \mathcal{M}_{21}^l p'_l + \mathcal{M}_{22}^l x'_l, \quad (23b)$$

$$p_r \approx \bar{p}_r + \mathcal{M}_{11}^r p'_r + \mathcal{M}_{12}^r x'_r, \quad (24a)$$

$$x_r \approx \bar{x}_r + \mathcal{M}_{21}^r p'_r + \mathcal{M}_{22}^r x'_r. \quad (24b)$$

The expansion coefficients are the elements of the total stability matrices \mathcal{M}^l and \mathcal{M}^r , as defined in Appendix A.

The classical actions in Eq. (20) can also be expanded about the two orbits, or guiding trajectories, thus providing

an analytical dependence on the initial and final coordinates:

$$S_l(x_l, x'_l) \approx \bar{S}_l + \bar{p}_l(x_l - \bar{x}_l) + \frac{\mathcal{M}_{11}^l}{2\mathcal{M}_{21}^l}(x_l - \bar{x}_l)^2 + \frac{\mathcal{M}_{22}^l}{2\mathcal{M}_{21}^l}(x'_l)^2 - \frac{1}{\mathcal{M}_{21}^l}(x_l - \bar{x}_l)x'_l, \quad (25a)$$

$$S_r(x_r, x'_r) \approx \bar{S}_r + \bar{p}_r(x_r - \bar{x}_r) + \frac{\mathcal{M}_{11}^r}{2\mathcal{M}_{21}^r}(x_r - \bar{x}_r)^2 + \frac{\mathcal{M}_{22}^r}{2\mathcal{M}_{21}^r}(x'_r)^2 - \frac{1}{\mathcal{M}_{21}^r}(x_r - \bar{x}_r)x'_r. \quad (25b)$$

The above expansions rely on the localization of the initial state. Inserting them into Eq. (20) and performing the integrations, the generating function transforms into a Gaussian quadrature

$$\langle x_l | \bar{\rho}_i^{(3)} | x_r \rangle \approx \left(\frac{\alpha - \gamma}{2\pi\hbar^2 \det A} \right)^{1/2} |\mathcal{M}_{21}^l \mathcal{M}_{21}^r|^{-1/2} \times \exp[\kappa_0 + \frac{1}{4}\mathbf{B} \cdot \mathbf{A}^{-1} \cdot \mathbf{B}], \quad (26)$$

where

$$\mathbf{B} = \left(-\frac{i}{\hbar \mathcal{M}_{21}^l}(x_l - \bar{x}_l), \frac{i}{\hbar \mathcal{M}_{21}^r}(x_r - \bar{x}_r) \right), \quad (27)$$

$$A = \begin{pmatrix} \alpha - \frac{i\mathcal{M}_{22}^l}{2\hbar \mathcal{M}_{21}^l} & -\gamma \\ -\gamma & \alpha + \frac{i\mathcal{M}_{22}^r}{2\hbar \mathcal{M}_{21}^r} \end{pmatrix}, \quad (28)$$

$$\kappa_0 = \frac{i}{\hbar}(\bar{S}_l - \bar{S}_r) + \frac{i}{\hbar} \bar{p}_l(x_l - \bar{x}_l) - \frac{i}{\hbar} \bar{p}_r(x_r - \bar{x}_r) + \frac{i\mathcal{M}_{11}^l}{2\hbar \mathcal{M}_{21}^l} \times (x_l - \bar{x}_l)^2 - \frac{i\mathcal{M}_{11}^r}{2\hbar \mathcal{M}_{21}^r} (x_r - \bar{x}_r)^2 - \frac{i\pi}{2}(\mu_l + \delta_l - \mu_r - \delta_r). \quad (29)$$

Upon reduction of Eq. (20) to Gaussian quadrature we have not only expanded the actions quadratically about the two guiding trajectories but also assumed that the prefactor to the exponent is constant over the entire domain. This is certainly a good approximation for a narrow Gaussian. The exponential function in Eq. (20) varies rapidly relative to the prefactor which represents the classical probability. This probability is also calculated along the two guiding orbits: \mathcal{M}^r and \mathcal{M}^l in the previous equations are the total stability matrices along the guiding orbits for the right and left propagation, respectively.

Equation (26) is simple to interpret and to implement. All the information required to determine the generating function is contained in the classical dynamics of two orbits launched at the center of the initial density matrix. The generating function gives the time evolution of this initial density matrix under the left–right propagators. The pair of clas-

sical orbits serve as a guiding phase space path for the dynamics of the density matrix; one orbit represents the evolving bra and the other represents the ket. As a consequence of the quadratic expansions of the classical dynamics and actions, the generating function is a Gaussian function at all times centered at \bar{x}_l, \bar{x}_r . This is precisely the limitation of this two-orbit implementation: The current expansions are exact for harmonic potentials but only apply in general anharmonic systems for relatively short times. Later we will analyze this method and its limitations with an example; we will also describe a generalization of the semiclassical propagation that is not restricted to short times.

V. THE THIRD-ORDER RESPONSE FUNCTION

So far we have introduced the semiclassical limit of the perturbative terms in the expansion of the density matrix for a system interacting with an external electromagnetic field. The generating functions previously calculated are an intermediate step for the determination of a physical observable. The trace of the dipole moment operator over the evolving density matrix yields the polarization of the chromophore under the influence of the electric field. Now let us introduce the response functions $S^{(1)}, S^{(2)}, S^{(3)}$:²

$$P^{(0)}(t) = \text{Tr}[\hat{\mu}\rho^{(0)}(-\infty)], \quad (30a)$$

$$P^{(1)}(t) = \int_0^{+\infty} dt_1 S^{(1)}(t_1)E(t-t_1), \quad (30b)$$

$$P^{(2)}(t) = \int_0^{+\infty} dt_2 \int_0^{+\infty} dt_1 S^{(2)}(t_2, t_1)E(t-t_2-t_1) \times E(t-t_2), \quad (30c)$$

$$P^{(3)}(t) = \int_0^{+\infty} dt_3 \int_0^{+\infty} dt_2 \int_0^{+\infty} dt_1 S^{(3)}(t_3, t_2, t_1) \times E(t-t_3-t_2-t_1)E(t-t_2-t_1)E(t-t_1). \quad (30d)$$

$S^{(1)}(t_1)$ is the linear response of the system which controls the linear optical measurements. $S^{(2)}(t_1, t_2)$ and $S^{(3)}(t_1, t_2, t_3)$ are the second and third order nonlinear response functions, respectively, which describe nonlinear optical measurements. Comparison of equations Eqs. (30) with Eqs. (7) and Eqs. (10) determines the response functions in terms of the generating functions $\bar{\rho}_k^{(n)}$:

$$S^{(1)}(t_1) = \left(\frac{i}{\hbar}\right) [J(t_1) - \text{c.c.}], \quad (31a)$$

$$S^{(2)}(t_2, t_1) = \left(\frac{i}{\hbar}\right)^2 \left[\sum_{j=1}^2 Q_j(t_2, t_1) + \text{c.c.} \right], \quad (31b)$$

$$S^{(3)}(t_3, t_2, t_1) = \left(\frac{i}{\hbar}\right)^3 \left[\sum_{j=1}^4 R_j(t_3, t_2, t_1) - \text{c.c.} \right], \quad (31c)$$

where

$$J(t_1) = \text{Tr}[\hat{\mu}\bar{\rho}^{(1)}(t-t_1; t)], \quad (32a)$$

$$Q_1(t_2, t_1) = -\text{Tr}[\hat{\mu}\bar{\rho}_1^{(2)}(t-t_2-t_1, t-t_1; t)], \quad (32b)$$

$$Q_2(t_2, t_1) = \text{Tr}[\hat{\mu}\bar{\rho}_2^{(2)}(t-t_2-t_1, t-t_1; t)], \quad (32c)$$

$$R_1(t_3, t_2, t_1) = \text{Tr}[\hat{\mu}\bar{\rho}_1^{(3)}(t-t_3-t_2, t-t_3, t-t_3-t_2-t_1; t)], \quad (32d)$$

$$R_2(t_3, t_2, t_1) = \text{Tr}[\hat{\mu}\bar{\rho}_1^{(3)}(t-t_3-t_2-t_1, t-t_3, t-t_3-t_2; t)], \quad (32e)$$

$$R_3(t_3, t_2, t_1) = \text{Tr}[\hat{\mu}\bar{\rho}_1^{(3)}(t-t_3-t_2-t_1, t-t_3-t_2, t-t_3; t)], \quad (32f)$$

$$R_4(t_3, t_2, t_1) = \text{Tr}[\hat{\mu}\bar{\rho}_2^{(3)}(t-t_3-t_2-t_1, t-t_3-t_2, t-t_3; t)]. \quad (32g)$$

The time variables chosen for the response functions are the time intervals between interactions t_i rather than the actual interaction times. As we see in Eqs. (32) the functions J , Q_j , and R_j are obtained through the tracing of the transition dipole moment and the generating functions. The total third-order response is the sum of four traces, each of them is associated to a particular pathway in Liouville space symbolized by the double-sided Feynman diagram, Fig. 1. The semiclassical approximation to the traces [Eqs. (32)] can be obtained by substituting the generating functions by the semiclassical expression derived in the previous section, Eq. (26). Although in Sec. IV we derived the two-orbit semiclassical expansion of the third-order generating functions, $\bar{\rho}_i^{(3)}$, in fact that formula equally applies to the second and linear order generating functions; the only change between the three cases is the number and sequence of quantum propagators in $\hat{\mathcal{U}}_i^r, \hat{\mathcal{U}}_i^l$. Consequently the recipe for describing the evolution of the classical orbits changes among the different generating functions due to the modification of the time evolution operators for the density matrix.

The interpretation of the nonlinear response provides a new physical insight into the dynamics. Each J , R_j , and Q_j depend on the time evolution of the density matrix and in particular they look for the “survival probability”, i.e., the probability of finding the system in the same region of configuration space after the left–right propagation. For this reason the semiclassical limit allows us to look at the guiding orbits that carry the flux of quantum probability amplitude through phase space back to the initial domain and understand the dynamical mechanism for correlations in complicated nonlinear systems. Since the transition dipole moment is set to unity the traces Eqs. (32) are simply the traces of the generating functions; in the case of the third-order terms

$$R_j(t_1, t_2, t_3) = \int dx \langle x | \bar{\rho}_i^{(3)} | x \rangle, \quad j=1, \dots, 4, \quad i=1, 2. \quad (33)$$

Using Eq. (26) then

$$\lim_{\hbar \rightarrow 0} R_j(t_3, t_2, t_1) \approx \sqrt{\frac{2(\alpha - \gamma)}{\pi}} \left(\text{sign} \frac{(\mathcal{M}_{21}^r \mathcal{M}_{21}^l)}{g} \right)^{1/2} \times \left(\frac{\pi}{k_2} \right)^{1/2} \exp \left[k_0 + \frac{k_1^2}{4k_2} \right]. \quad (34)$$

All the quantities appearing in Eq. (34) are defined in Appendix B. The “sign” function refers to the sign of the dependent variable. R_j ends up depending only on the information of the two guiding classical orbits.

It is possible to express the second- and third-order terms Q_j and R_j as multiple time correlation functions of the transition dipole. By explicitly writing the generating functions in terms of the quantum propagators, one visualizes them in terms of averages of physical quantities like the transition dipole moment

$$Q_1(t_2, t_1) = -\langle \hat{\mu}(t-t_2) \hat{\mu}(t) \hat{\mu}(t-t_2-t_1) \rho^{(0)}(-\infty) \rangle, \quad (35a)$$

$$Q_2(t_2, t_1) = \langle \hat{\mu}(t) \hat{\mu}(t-t_2) \hat{\mu}(t-t_2-t_1) \rho^{(0)}(-\infty) \rangle, \quad (35b)$$

$$R_1(t_3, t_2, t_1) = \langle \hat{\mu}(t-t_3-t_2) \hat{\mu}(t-t_3) \hat{\mu}(t) \hat{\mu}(t-t_3-t_2-t_1) \rho^{(0)}(-\infty) \rangle, \quad (35c)$$

$$R_2(t_3, t_2, t_1) = \langle \hat{\mu}(t-t_3-t_2-t_1) \hat{\mu}(t-t_3) \hat{\mu}(t) \hat{\mu}(t-t_3-t_2) \rho^{(0)}(-\infty) \rangle, \quad (35d)$$

$$R_3(t_3, t_2, t_1) = \langle \hat{\mu}(t-t_3-t_2-t_1) \hat{\mu}(t-t_3-t_2) \hat{\mu}(t) \hat{\mu}(t-t_3) \rho^{(0)}(-\infty) \rangle, \quad (35e)$$

$$R_4(t_3, t_2, t_1) = \langle \hat{\mu}(t) \hat{\mu}(t-t_3) \hat{\mu}(t-t_3-t_2) \hat{\mu}(t-t_3-t_2-t_1) \rho^{(0)}(-\infty) \rangle. \quad (35f)$$

Equation (34) is exact for purely harmonic surfaces. Since the semiclassical propagators and the stationary phase approximation are exact in this case, this formula also applies for the calculation of the second-order responses Q_j .

When the potential surfaces are anharmonic, Eq. (34) yields a good estimate of the dynamics up to the time when the nonlinear dynamics starts to create multiple simultaneous classical recurrences in the response functions R_j . The recurrences in R_j appear because at certain time t there are classical paths that take amplitude from the initial density matrix back to itself. This must happen simultaneously for the left and right propagation. In the case of a harmonic oscillator the dynamics is very simple: only one orbit on the left and one on the right can bring amplitude simultaneously back to the initial density matrix creating a recurrence [see Fig. 4(a)]. However, for anharmonic systems more than one pair of orbits can contribute at the same time to create a recurrence in the correlation functions. Therefore, by that time, Eq. (34) would not be valid because we have essen-

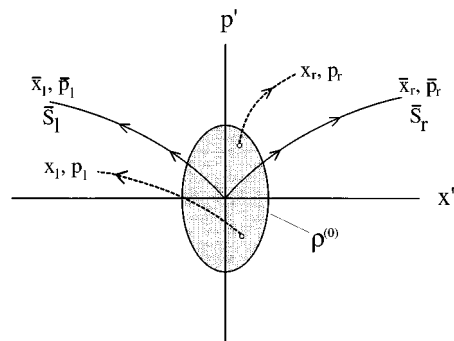


FIG. 3. Notation used in the two-orbit semiclassical expansion of the generating functions. Solid lines are the central guiding orbits and the dash lines are two arbitrary orbits in the neighborhood of the center of $\rho^{(0)}$.

tially used linearization of the classical dynamics about a single orbit per propagator. Nonlinear effects in the dynamics require linearization about more than one orbit,²⁰ Fig. 4(b).

VI. APPLICATION TO A TWO ELECTRONIC LEVEL SYSTEM

After introducing the response function formalism and its semiclassical implementation we are ready to apply this machinery to a test model. Let us consider a two electronic level molecular system with one nuclear degree of freedom described by the following Hamiltonian

$$H_0 = h_1(x) |1\rangle\langle 1| + h_2(x) |2\rangle\langle 2| - \hat{\mu}_{12} \cdot E(t) |1\rangle\langle 2| - \hat{\mu}_{21} \cdot E(t) |2\rangle\langle 1|. \quad (36)$$

x is the coordinate degree of freedom, e.g., an internuclear distance, and μ_{ij} the dipole transition moment coupling the Born–Oppenheimer surfaces i, j . In Eq. (36) h_1 and h_2 are the Hamiltonians for the two electronic surfaces. Although the tensor nature of the field–system interaction is clear we will not address it. For the sake of clarity we assume that the field is aligned with the dipole moment of the chromophore, we can then write in scalar notation the interaction as $\hat{\mu}_{ij} E(t)$.

For the two-level system considered here the lowest nonlinear term in the polarization is the third-order one. $P_2(t)$ is identically zero. Substitution of Eq. (36) in Eqs. (8e) and (8d) gives for the lower order nonlinear contribution

$$\bar{\rho}_1^{(3)}(t) = e^{-ih_2(t-\tau_3)/\hbar} e^{-ih_1\tau_3/\hbar} \rho^{(0)}(-\infty) \times e^{ih_1\tau_1/\hbar} e^{ih_2(\tau_2-\tau_1)/\hbar} e^{ih_1(t-\tau_2)/\hbar}, \quad (37a)$$

$$\bar{\rho}_2^{(3)}(t) = e^{-ih_2(t-\tau_3)/\hbar} e^{-ih_1(\tau_3-\tau_2)/\hbar} e^{-ih_2(\tau_2-\tau_1)/\hbar} \rho^{(0)}(-\infty) e^{ih_1t/\hbar}. \quad (37b)$$

As explained in a previous section, under the Condon approximation the dipole transition moments are constant with respect to nuclear motions and we set $\hat{\mu}_{ij} = 1$. Conse-

TABLE II. Explicit expressions for the left and right operators appearing in the third-order response.

$\hat{\rho}_r^2 = e^{ih_1t/\hbar}$
$\hat{\rho}_l^2 = e^{-ih_2(t-\tau_3)/\hbar} e^{-ih_1(\tau_3-\tau_2)/\hbar} e^{-ih_2(\tau_2-\tau_1)/\hbar} e^{-ih_1\tau_1/\hbar}$
$\hat{\rho}_r^1 = e^{ih_1\tau_1/\hbar} e^{ih_2(\tau_2-\tau_1)/\hbar} e^{ih_1(t-\tau_2)/\hbar}$
$\hat{\rho}_l^1 = e^{-ih_2(t-\tau_3)/\hbar} e^{-ih_1\tau_3/\hbar}$

quently the equations for the generating functions [Eqs. (37)] are simply given by products of time evolution operators in lower and upper electronic states.

In Table II we have summarized the left and right operators, $\hat{\mathcal{U}}_i^l$ and $\hat{\mathcal{U}}_i^r$, for this system that yield the third-order response function from the time evolution of the initial density matrix.

The terms that determine the third-order polarization via Eq. (30) can be also written as

$$R_j(t_1, t_2, t_3) = \int dx \int dx'_i dx'_r \langle x | \hat{\mathcal{U}}_i^l | x'_i \rangle \langle x'_i | \rho^{(0)}(-\infty) | x'_r \rangle \langle x'_r | \hat{\mathcal{U}}_i^r | x \rangle, \quad (38)$$

$j=1, \dots, 4, \quad i=1, 2.$

$\hat{\mathcal{U}}_i^r$ and $\hat{\mathcal{U}}_i^l$ can be thought as the bra and ket time evolution operators for the third order term. We have already pointed out that expressing these operators as a product of Van Vleck propagators, Eq. (14), unfortunately leads to the generation of a ‘‘cascade’’ of orbits. In Sec. III we also introduced the notion of calculating by stationary phase approximation the classical paths that take the system from initial to final position through the transitions between electronic levels. The final formula for R_j [Eq. (34)] has a structure very similar to the Van Vleck propagator, Eq. (14).

As an example for the calculation of the δ index let us calculate the explicit form of $\langle x'_r | \hat{\mathcal{U}}_r^2 | x_r \rangle$. Substitution of the Van Vleck formula gives

$$\langle x'_r | \hat{\mathcal{U}}_r^2 | x_r \rangle = \int dx_1 \langle x'_r | e^{ih_1\tau_3/\hbar} | x_1 \rangle \langle x_1 | e^{ih_2(t-\tau_3)/\hbar} | x_r \rangle \quad (39a)$$

$$\approx -\frac{1}{2\pi i\hbar} \int dx_1 \left| \frac{\partial^2 S_1}{\partial x'_r \partial x_1} \right|^{1/2} \left| \frac{\partial^2 S_2}{\partial x_1 \partial x_r} \right|^{1/2} \times \exp \left[-\frac{i}{\hbar} (S_1 + S_2) + \frac{i\pi}{2} (\mu_1 + \mu_2) \right]. \quad (39b)$$

The actions are calculated along the classical orbits joining (x'_r, x_1) and (x_1, x_r) in times τ_3 , $t - \tau_3$, respectively. The two classical orbits are disconnected because they come from two separate roots to independent boundary conditions. This poses a problem because the use of the propagator Eq. (39b) requires launching two separate manifolds of orbits: one at x'_r with arbitrary momentum and another at x_1 also with all possible values of initial momentum. However, as $\hbar \rightarrow 0$ the main contribution to the integral Eq. (39b) is a classically connected orbit, whereby momentum and position are preserved when switching propagators. We reach this conclusion by calculating the integral above by stationary phase:

$$\langle x'_r | \hat{\mathcal{U}}_r^2 | x_r \rangle \approx (-2\pi i\hbar)^{-1/2} \left| \frac{\partial^2 S_T}{\partial x_r \partial x'_r} \right|^{1/2} \times \exp \left[-\frac{i}{\hbar} S_T(x_r, x'_r) + \frac{i\pi}{2} (\mu + \delta) \right], \quad (40)$$

where we have made use of the following equalities

$$\left| \frac{\partial^2 S_T}{\partial x_r \partial x'_r} \right|^{1/2} = \left| \frac{\partial^2 S_1}{\partial x'_r \partial x_1} \right|^{1/2} \left| \frac{\partial^2 S_2}{\partial x_r \partial x_1} \right|^{1/2} \left| \frac{\partial^2 (S_1 + S_2)}{\partial x_1^2} \right|^{1/2}, \quad (41a)$$

$$S_T = S_1 + S_2, \quad (41b)$$

$$\mu = \mu_1 + \mu_2. \quad (41c)$$

$S_T(x_r, x'_r)$ is the total action accumulated along a classical path going from x'_r to x_r preserving position and momentum when passing from the electronic surface 2 to 1 (notice that the orbits run forward in time). The index μ (a total Morse index) is the sum of conjugate points found along the two classical orbits in the path μ_1 and μ_2 .

As important is the new phase shift δ emerging from the stationary phase approximation and due to the discontinuity of the semiclassical propagation. This index arises when imposing the connectivity condition in the quantum paths joining x'_r and x_r . δ can be calculated by using the stability matrices of both classical fragments, $M^{(1)}$ and $M^{(2)}$ (see Appendix A). By definition

$$\begin{pmatrix} dp_1 \\ dx_1 \end{pmatrix} = M^{(1)} \begin{pmatrix} dp'_r \\ dx'_r \end{pmatrix}, \quad (42)$$

$$\begin{pmatrix} dp_r \\ dx_r \end{pmatrix} = M^{(2)} \begin{pmatrix} dp_1 \\ dx_1 \end{pmatrix}. \quad (43)$$

Then

$$\begin{cases} \delta = 0 & \text{if } M_{22}^{(1)}/M_{21}^{(1)} + M_{11}^{(2)}/M_{21}^{(2)} \geq 0 \\ \delta = 1 & \text{if } M_{22}^{(1)}/M_{21}^{(1)} + M_{11}^{(2)}/M_{21}^{(2)} < 0. \end{cases} \quad (44)$$

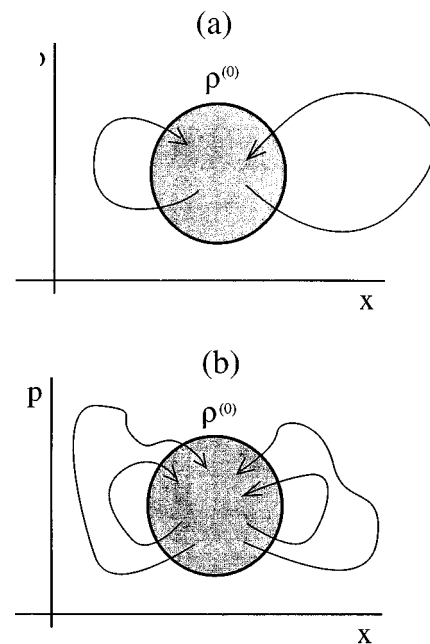


FIG. 4. Phase space diagram showing the initial density matrix $\rho^{(0)}(-\infty)$ (shaded area) and the classical left and right guiding orbits. In case (a) only one family of orbits serves as guide for the time evolution. In case (b) two families of orbits guide the dynamics creating a recurrence in the correlation function.

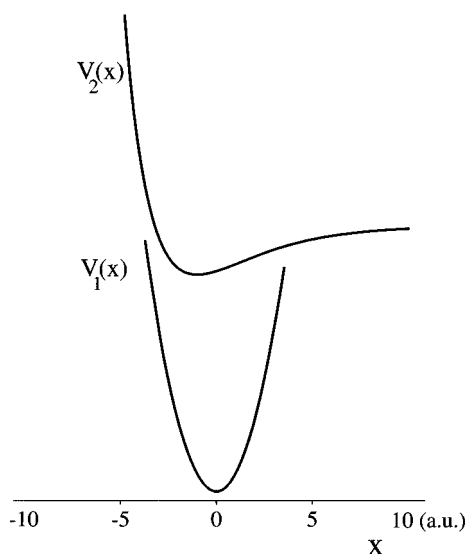


FIG. 5. Model two level system: The ground state is a harmonic potential, the excited state is a Morse potential. Both curves are drawn as a function of an internuclear distance x .

This new stationary phase approximation is very important because it avoids relaunching an x -manifold of orbits at x_1 to calculate the second semiclassical propagation. We can then send a ray of orbits started at x'_r with different initial momentum and let them go through the electronic surface change until they reach their final destination at x .

We now present a numerical example of the semiclassical two-orbit method described and compare the semiclassically calculated third-order nonlinear response with its quantum counterpart, calculated using a standard numerical algorithm.

Consider a two electronic level system with a harmonic ground state and a Morse excited state. The Hamiltonians h_1, h_2 in Eq. (36) are then given by

$$h_1(x) = \frac{p^2}{2m} + \frac{1}{2} m\omega^2 x^2, \quad (45a)$$

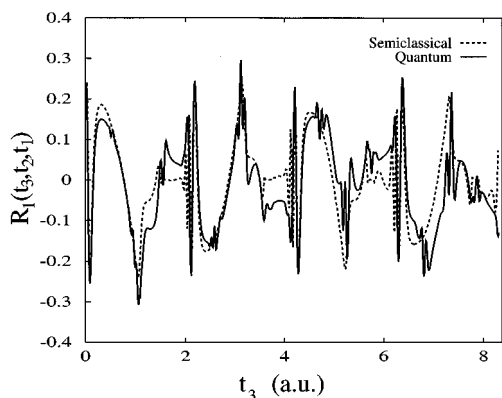


FIG. 6. Third order trace R_1 as a function of t_3 for fixed $t_1=0.59$ and $t_2=0.61$ (a.u.).

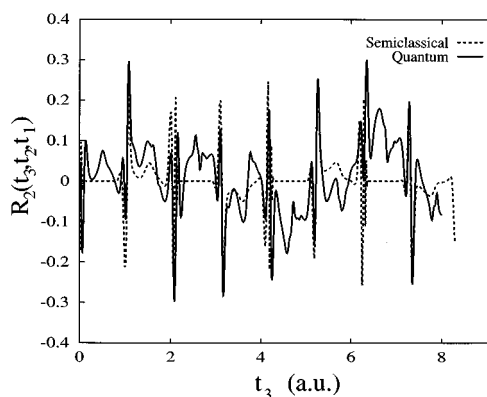


FIG. 7. Third order trace R_2 as a function of t_3 for fixed $t_1=0.59$ and $t_2=0.61$ (a.u.).

$$h_2(x) = \frac{p^2}{2m} + D_e(1 - \exp[-\alpha_e(x-x_e)])^2 + E_{ge}, \quad (45b)$$

where $m=1$, $\omega=6.0$ for the ground state harmonic oscillator and $D_e=50$, $x_e=-1$, $\alpha_0=0.3086$ for the first excited state Morse potential (see Fig. 5). The electronic energy difference between the two surfaces E_{ge} leads to an overall oscillatory contribution to the traces R_j , $j=1, \dots, 4$. To better appreciate the agreement between semiclassical and quantum results in the following figures we have made this constant factor zero.

The system starts at equilibrium in the harmonic state with $kT=10\hbar\omega$; k being Boltzman's constant and using atomic units $\hbar=1$. In Figs. 6–9 we have plotted the four traces that constitute the third-order response $S^{(3)}$ as a function of t_3 . The other two time variables t_1 and t_2 were fixed to 0.59 and 0.61 a.u., respectively. The last time interval t_3 describes the evolution of an electronic coherence between the ground and excited states and by letting it vary we see the agreement of the semiclassical two-orbit approximation with the quantum as a function of time. The quantum calculations were performed using a FFT–Feit–Fleck implementation of the Liouville–Von Neuman equation.²³ The figures show a reasonable agreement; R_1 , R_4 , and R_2 happen to be better described by the two-path expansion than R_3 . In all cases the simple semiclassical approximation works almost

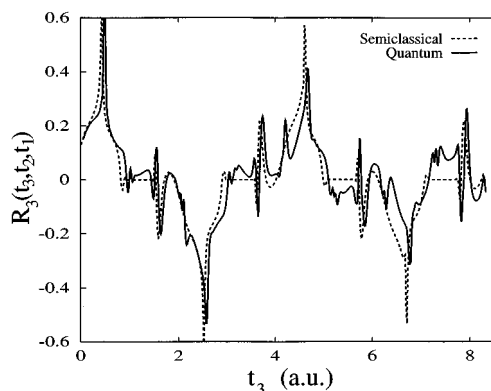


FIG. 8. Third order trace R_3 as a function of t_3 for fixed $t_1=0.59$ and $t_2=0.61$ (a.u.).

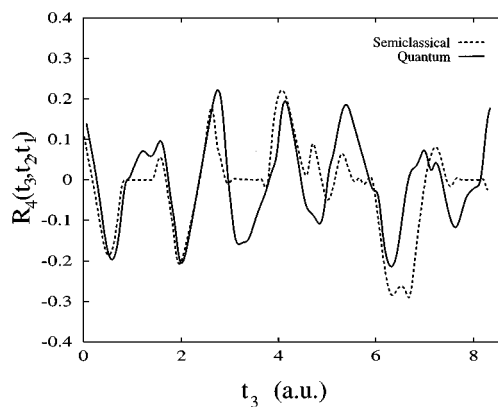


FIG. 9. Third order trace R_4 as a function of t_3 for fixed $t_1=0.59$ and $t_2=0.61$ (a.u.).

exactly at short times and it gets worse at longer times. As mentioned before, expanding the dynamics about only two classical orbits takes the risk of neglecting contributions to the correlation functions from classical paths that make a long excursion far from our guiding orbits. Nevertheless this method remains extremely useful for relatively short time dynamics; the difference in computational effort between the quantum and the two-path semiclassical calculations is astonishing. The FFT calculation of the R_j 's took several hours of CPU on a workstation while the semiclassical two-path took seconds on the same machine. One of the inconveniences of the FFT method for this particular problem is the necessity of propagating the density matrix using two potential surfaces with very different coordinate intervals. In the present example the harmonic potential is rather narrow in coordinates while the Morse potential is extended.

Using the semiclassical approximation it is also possible to depict in phase space the classical path followed by the density matrix for each of the terms R_1, \dots, R_4 . Each term can be described using three pictures (see Figs. 10–13): To the upper left and lower right is shown the left and right guiding orbits, respectively, in phase space, in the lower left the configuration space trajectory described by the density matrix is also plotted by interpolating the coordinate excursions

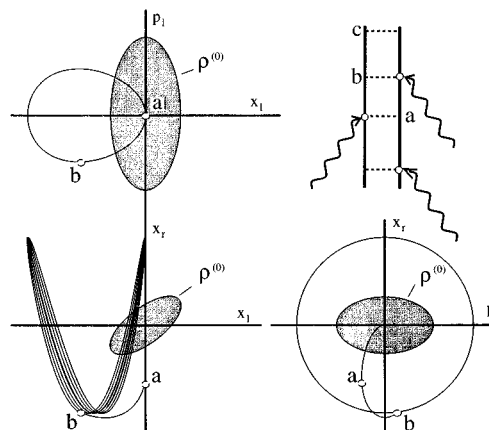


FIG. 11. Phase space portrait of the classical guiding orbits for R_2 .

from the left and right classical orbits. When the density matrix is represented in the coordinate representation (x_l, x_r) it appears as if its time evolution follows a two-dimensional space; it would seem ideal to obtain equations of motion for the evolution in (x_l, x_r) of the center of the moving density matrix. However in reality this density matrix is evolving in a four-dimensional space that contains the left and right momenta as well. This is precisely what is shown in Figs. 10–13; the left and right guiding orbits explore the classical dynamics of the density matrix in its full dimensionality while the projection of the simultaneous left–right positions gives the path described by the density matrix in the coordinate representation. For the current example, these paths obviously correspond to a regular integrable motion. We have used white circles and the labels a, b, c to show the positions of the classical guiding orbits after the t_1, t_2 , and t_3 propagations. Notice that the equations of motion change abruptly at times t_1 and t_2 , and so does the structure of the classical guiding orbits. The right guiding paths for the response functions R_1, R_2, R_3 are made of two classical orbits, the first one running on the excited Morse state and the second one on the ground harmonic potential. On the other hand the left guiding path runs along the upper Morse potential. Both guiding paths classically describe an

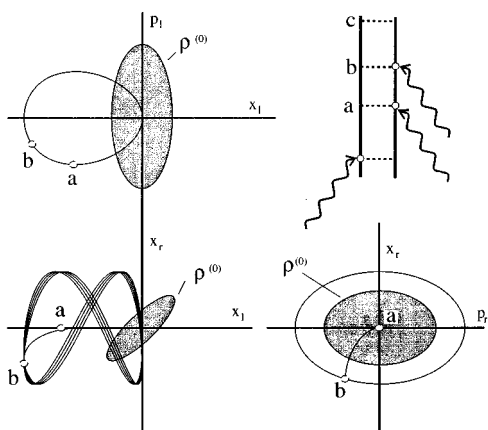


FIG. 10. Phase space portrait of the classical guiding orbits for R_1 .

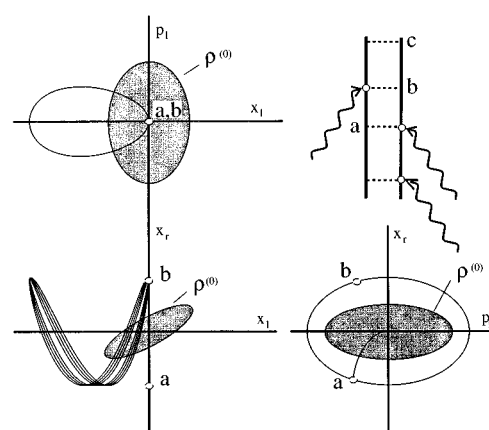


FIG. 12. Phase space portrait of the classical guiding orbits for R_3 .

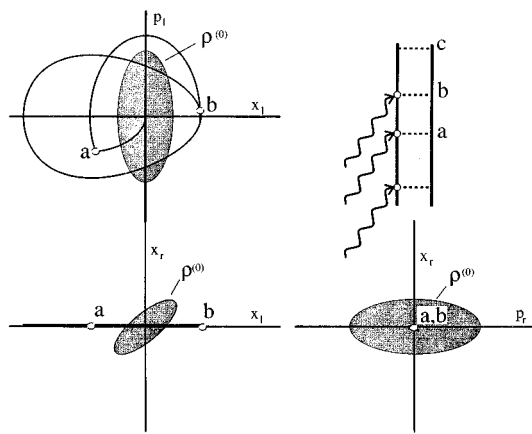


FIG. 13. Phase space portrait of the classical guiding orbits for R_4 .

electronic coherence created by the three field interactions. In the remaining response function R_4 the three interactions occur on the left-hand side of the density matrix (see Fig. 1). The phase space diagram of R_4 (Fig. 13) then shows a left guiding path with three classical orbits; the first one running on the Morse potential, the second on the harmonic ground state, and the third one again on the upper Morse. The right guiding orbit is simply a stationary point at the origin because the lack of field interaction leaves the classical orbit stationary at the minimum of the harmonic potential.

The phase space picture for the dynamics of the density matrix provides a quick and inexpensive way to visualize and predict the response functions. Since the nonlinear response functions are given by the traces of the time evolved density matrix, $\tilde{\rho}_{1,2}^{(3)}$, only the configuration space region along the $x_l = x_r$ axis is important. When the density matrix passes through this axis it is expected to give a recursion in the trace. Similarly, the amplitude of the trace should become negligible far from the $x_l = x_r$ axis. There is a second important factor for using classical phase space diagrams; if the classical path (x_l, x_r) crosses the diagonal $x_l = x_r$ but the momentum of either of the right-left orbits is too high then the trace can be small. This is easily understandable: The classical path in configuration space (left-bottom plot in Figs. 10–13) describes the motion of the center of the density matrix only, it does not tell us about the overall average momentum of the moving distribution. If the average momentum of the density matrix is very high then $\tilde{\rho}_{1,2}^{(3)}$ will exhibit large fringes and its trace over the $x_l = x_r$ may show negligible results.

To explore the insight classical mechanics gives into the nonlinear responses let us look at the term R_4 for two different sets of times t_1, t_2 , again as a function of t_3 . In Fig. 14 the traces R_4 for $t_1 = 0.39$, $t_2 = 1.6$, and $t_1 = 0.59$, $t_2 = 1.4$ are shown. In the case of R_4 the trace is determined by the left orbit because the right orbit corresponds to the equilibrium point on the harmonic potential. The classical paths plotted in the figure have three segments, one for each of the t_i propagations. The path of the first run makes a very short excursion around the $x_l = 0$, $p_l = 0$ point while for the second run it is evident that the classical path described during the

t_3 interval is much larger. The right orbit stays at $x_r = 0$ (the harmonic stationary point). Therefore only when x_l is also equal to 0, at the p_l axis, can the trace of R_4 be significant. There are only two points per period where there is an intersection between the Morse orbit and the p_l axis, and in both points the momentum of the guiding orbit is nonzero. As a result the traces should be expected to be small; also the higher the momentum at the crossing the smaller the trace. We can observe this effect in the plot, the run for the second set of parameters is described by a guiding orbit which intersects the $x_l = 0$ condition with a very large momentum (large or small momentum here means far or close to the average initial momentum).

In summary the two-orbit semiclassical approximation to the propagation of the density matrix provides an efficient way to visualize the regions of phase space explored by the evolving distribution, and examine the left and the right sides of the propagation separately. The diagrams in Figs. 10 to 13 show then the classical guiding orbits underlying the nonlinear response contributions R_1 , R_2 , R_3 , and R_4 . The paths in configuration space (x_l, x_r) (lower-left) allow one to see when to expect an increase in the trace of the nonlinear response. Similarly the phase space projections to the left and right allow one to read the average momentum of the density matrix as it crosses the diagonal $x_l = x_r$.

The numerical effort involved in the two-orbit semiclassical calculation of R_j $j = 1, \dots, 4$ is very small. For this reason it is rather easy to explore the behavior of the nonlinear response functions in their multidimensional space t_1, t_2, t_3 . One of the advantages of the nonlinear optical response is that these functions provide a unified picture for many different spectroscopic measurements. For example, a normal two-photon echo experiment is described by the function $R_2(t_1, 0, t_3)$ where t_1 is the time difference between the two light pulses and t_3 the time interval between the last pulse and the echo detection. Along the $t_1 = t_3$ direction it is possible to eliminate the inhomogeneous broadening that hinders the measurement of spectral lines in a normal linear absorption spectra. Using our semiclassical expansion we can now calculate with small numerical effort $R_2(t_1, 0, t_3)$ as a function of both t_1, t_3 . Figure 15 shows a contour plot of the absolute value of the nonlinear response R_2 for our harmonic Morse model, we may as well call it the photon-echo response, as a function of t_1 and t_3 . The time intervals range from 0 to 6 a.u. Two clear kinds of recurrences emerge in the response that we have labeled A and B. Departing from the origin and following the $t_1 = t_3$ diagonal we first observed an immediate decay of the trace R_2 followed by a sequential series of recurrences of type B, A, B, etc. Each of the recurrences can be identified with particular classical paths that involve combinations of periods of motion in the Morse and harmonic surfaces. The signal, which is an electronic coherence, will depend on a combination of motions on both surfaces. Let us first analyze recurrence type A with the help of the Feynman diagram shown at the bottom right of Fig. 15. During the t_1 interval, i.e., after the interaction with first pulse, the bra side of the density matrix (right path) has been excited to the upper Morse potential while the ket side (left) remains in the ground harmonic. The contour plot shows that

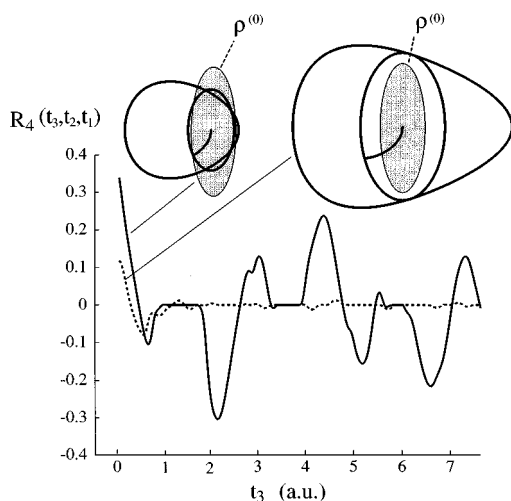


FIG. 14. Comparison of two runs for $R_4(t_3, t_2, t_1)$ for fixed t_1, t_2 as a function of t_3 . In the upper two diagrams the phase space picture (p_l, x_l) of the classical path described by the left propagation can be compared with their respective correlation functions R_4 .

for $t_3=0$ and as t_1 increases the response first decays and then rebuilds in a series of type A recurrences. The moment when this happens for the first time coincides with the first period of motion of the right Morse orbit. Even if the t_1 motion continues on forever, the left guiding orbit remains stationary at $x_l=0, p_l=0$. This means that only when the right orbit goes through $x_r=0$ with small or zero momentum there will be a recurrence ‘‘A’’ in the trace. The events ‘‘A’’ happen along the $t_3=0$ axis periodically (at least for t_1 from 0 to 6.0) due to the periodic motion of the moving density matrix along the Morse orbit. Similar argument applies along the $t_1=0$ axis.

The same kind of recurrence type A appears along the $t_3=t_1$ line, e.g., at the label A location. The classical reason for these recurrences is also easily found by looking at the phase space portraits of the left and right guiding orbits. Every one of these recurrences is due to the combination of an integer number of periods along the Morse orbit by the left and right guiding orbits. Because the Morse orbits have time to complete a full circuit in phase space they always bring the density matrix back to its departure position, thus almost completely rebuilding the trace.

In Fig. 16 we depict the classical guiding orbits for the recurrence labeled B. During the time interval t_1 the dynamics moves along the $t_3=0$ axis and we observe the initial decay of the trace, by the end of half-period in the Morse orbit of the right guiding path the density matrix has moved along the x_r axis (bottom-left diagram) away from the important diagonal $x_l=x_r$. As we mentioned, only when the guiding path crosses this diagonal the trace builds up once more. During the t_3 propagation the right orbit describes a full period of motion in the harmonic potential while the left orbit moves on the Morse excited state for half a period. As a result there are two intersections of (x_l, x_r) with the diagonal. The first fails to produce a recurrence in the response because the average momentum of the distribution is ex-

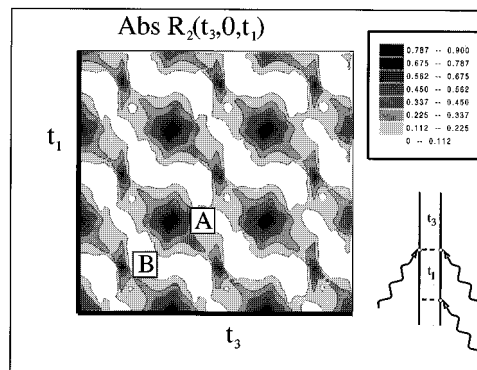


FIG. 15. Contour plot of the nonlinear response R_2 for a two photon echo measurement.

tremely high in the right orbit. The second intersection happens after one full period of the harmonic oscillator in the right orbit, and in this case the average momentum of the density matrix is zero (same as the initial value). Only at this moment is there a full revival of the trace. If the dynamics continue for longer t_3 , i.e., along the horizontal line in the R_2 contour plot, we see another couple of identical recurrences of type B which are again due to a combination of one full harmonic and half Morse periods.

The classical analysis identifies recurrences A purely associated with the dynamics on the Morse excited potential. This is precisely what is to be expected for a photoabsorption measurement and the trace of R_2 along the $t_1=0$ or $t_3=0$ axis is exactly that. Along the diagonal $t_1=t_3$ we have not only the information about the linear absorption spectrum (recurrence type A) but also a new kind of recurrence (type B) which is associated to a combination of dynamics in both the upper and lower electronic states.

As a corollary to this analysis we reiterate that this simple interpretation holds for the relatively short time scale shown in Fig. 15. For longer times the effect of the nonlinear dynamics in the Morse potential increases and a simple two-orbit expansion is not sufficient to describe the semiclassical dynamics. In that time domain one has to use a semiclassical implementation that makes use of the full dynamics in phase space, expanding the evolution of the density matrix along multiple classical orbits. In the following section we described such a method. However it is important to emphasize that the two-orbit expansion is much more powerful than one may think superficially; a possible alternative would be to expand the upper Morse potential quadratically and approximate it with another harmonic potential. This approximation is equivalent in our two-orbit picture to having guiding orbits that move on two harmonic surfaces; unfortunately the frequencies seen by the evolving orbits is always constant due to the global harmonic approximation to the potential. On the other hand our two-orbit approximation adjusts the frequency of the upper harmonic ‘‘fit’’ constantly, making it larger in the asymptotic side of the Morse potential and shorter close to its steep wall.

VII. MULTIPLE PATH SEMICLASSICAL EXPANSION OF THE NONLINEAR RESPONSE FUNCTION

The multiple path semiclassical expansion of the nonlinear response is based on the “cellular dynamics” method applied for the semiclassical propagation of Gaussian wave packets in general potentials.^{20,24,25}

We first write the quantum propagators for the ket and bra $\hat{\mathcal{U}}_l$ and $\hat{\mathcal{U}}_r$ in an initial value representation using a mixed coordinate-momentum representation. For instance, the left propagator can be written as

$$\langle x_2 | \hat{\mathcal{U}}_l | x_1 \rangle_{sc} \approx \int dp_2 \langle x_2 | p_2 \rangle \langle p_2 | \hat{\mathcal{U}}_l | x_1 \rangle, \quad (46a)$$

$$= (4\pi^2 i \hbar^2)^{-1/2} \int dp_1 |\mathcal{M}_{11}^l|^{1/2} \times \exp \left[\frac{i}{\hbar} S_l(x_1, p_1) + \frac{i}{\hbar} p_l(x_2 - x_1) - \frac{i\pi}{2} \phi \right]. \quad (46b)$$

In going from Eq. (46a) to Eq. (46b) we have substituted the element of matrix $\langle p_2 | \hat{\mathcal{U}}_l | x_1 \rangle$ by its semiclassical limit; the variable of integrations have also been changed using the classical stability matrix. $S_l(x_1, p_1)$ is the classical action accumulated along the left propagation that is launched at x_1, p_1 . x_t, p_t are the position and momentum of the classical orbit after time $t = (t_1, t_2, t_3)$ of propagation; they are also functions of the initial conditions x_1, p_1 . The phase factor ϕ , as explained in Ref. 25, accounts for the phase shifts across caustics in the mixed p - x representation

$$\phi = \mu_l + \delta_l + \frac{1}{2} \text{sgn}(-\mathcal{M}_{11}^l \mathcal{M}_{21}^l), \quad (47)$$

where μ_l is the total Morse index for the left path and δ_l the additional phase shift. A similar expression for the right propagator can be written in terms of an integral over initial momentum.

Propagators of the form [Eq. (46a)] easily allow one to recast the expression for the generating functions as an integral over initial momentum and position. In the case of the third-order generating functions

$$\langle x_l | \bar{\rho}_i^{(3)} | x_r \rangle \approx \int dx_1 dx_2 \langle x_l | \hat{\mathcal{U}}_l | x_1 \rangle_{sc} \times \langle x_1 | \rho^{(0)}(-\infty) | x_2 \rangle \langle x_2 | \hat{\mathcal{U}}_r | x_r \rangle_{sc}, \quad (48)$$

where the semiclassical propagators are now integrals over initial momentum:

$$\langle x_l | \hat{\mathcal{U}}_l | x_1 \rangle_{sc} = (4\pi^2 i \hbar^2)^{-1/2} \int dp_1 |\mathcal{M}_{11}^l|^{1/2} \times \exp \left[\frac{i}{\hbar} S_l(x_1, p_1) + \frac{i}{\hbar} p_l^l(x_l - x_1^l) - \frac{i\pi}{2} \phi_l \right], \quad (49a)$$

$$\langle x_2 | \hat{\mathcal{U}}_r | x_r \rangle_{sc} = (-4\pi^2 i \hbar^2)^{-1/2} \int dp_2 |\mathcal{M}_{11}^r|^{1/2} \times \exp \left[-\frac{i}{\hbar} S_r(x_2, p_2) - \frac{i}{\hbar} p_r^r(x_r - x_2^r) + \frac{i\pi}{2} \phi_r \right]. \quad (49b)$$

Due to the previous transformations the generating function can be expressed as a four-dimensional integral over the full phase space of initial conditions, both for the bra and the ket spaces.

In Sec. IV we showed how under certain circumstances the dynamics in the propagator could be expanded about a single pair of trajectories, one for the bra and one for the ket. This is equivalent to expanding the integrand of Eq. (48) about a single point in the phase space of initial conditions. The point chosen in the two-orbit expansion was logically, the average position and momentum of the initial density matrix. On the other hand, now we can go one step further; with the initial phase space representation it is possible to reduce the four-dimensional integration to an approximate sum over a set of grid points in (p_1, x_1, p_2, x_2) space. From each point in such a grid depart pairs of classical orbits which can be used for the local expansion of the integral [Eq. (48)] in exactly the same way as in the two-orbit implementation presented in Sec. IV.

A convenient way to transform the semiclassical expression for $\bar{\rho}_i^{(3)}$ to a sum over grid points in initial phase space is the insertion of a sum of localized states, Gaussians, in phase space. Consider the following representation of unity:

$$\sum_{i_1} \exp[-\beta_1(p_1 - p_{i_1})^2] \approx 1, \quad (50a)$$

$$\sum_{i_2} \exp[-\beta_2(x_1 - x_{i_2})^2] \approx 1, \quad (50b)$$

$$\sum_{i_3} \exp[-\beta_3(p_2 - p_{i_3})^2] \approx 1, \quad (50c)$$

$$\sum_{i_4} \exp[-\beta_4(x_2 - x_{i_4})^2] \approx 1. \quad (50d)$$

The widths of the Gaussians, β_i , and the centers $x_{i_2}, x_{i_4}, p_{i_1}, p_{i_3}$ can be chosen to make the sums as close to unity as desired. The set of points $(p_{i_1}, x_{i_2}, p_{i_3}, x_{i_4})$ define a grid in the phase space of initial conditions. Inserting the four sums in Eq. (48) then leads to a fourfold sum of integrals, however each of the integrands now are functions that decay very rapidly away from the center of the grid (provided that the β 's are sufficiently large). Then a quadratic expansion of the actions (S_l, S_r), as performed in Sec. IV about the grid point and the pair of classical orbits departing from it, reduces the integration problem to a simple Gaussian quadrature:

$$\langle x_l | \hat{\rho}_i^{(3)} | x_r \rangle \approx \left(\frac{\eta}{2\pi\hbar} \right)^2 \sqrt{\frac{2(\alpha-\gamma)}{\pi}} \sum_{i_1, \dots, i_4} |\mathcal{M}_{11}^l \mathcal{M}_{11}^r|^{1/2} \times \exp[\theta_0 + \frac{1}{4} \hat{\theta}_1 \cdot \hat{\theta}_2^{-1} \cdot \theta_1]. \quad (51)$$

The constant η is a normalization factor that insures the sum over Gaussians inserted in Eq. (48) to be approximately unity in phase space. Obviously the sum runs over all the grid points, each point in the grid is actually a couple of classical orbits. In practice it is not always necessary to insert unity as a sum over Gaussian in both coordinate and momenta, in the same case only a grid in coordinate will be sufficient and in other cases a grid in momenta space should be enough. For example, when the initial density matrix is very compact in configuration space (α large and high density of states) then the dynamics of the system can be clearly expanded only about the average position of $\rho^{(0)}$. However, a narrow initial state in coordinates implies very broad distribution of initial momenta; for this reason we cannot carry on the semiclassical propagation too far in time by expanding the dynamics only about the average momentum of the initial state, many pairs of orbits at different initial momenta

are necessary. This is precisely our case, we will insert only two sums over Gaussians [Eqs. (50a) and (50c)] which expand the initial momenta in a grid of points, then the coefficients θ take the following form

$$\theta_0 = -\alpha(\bar{x}'_r)^2 - \alpha(\bar{x}'_l)^2 + 2\gamma\bar{x}'_r\bar{x}'_l - \frac{i\pi}{2}(\phi_l - \phi_r) + \frac{i}{\hbar}(\bar{S}_l - \bar{S}_r) + \frac{i}{\hbar}\bar{p}_l(x_l - \bar{x}_l) - \frac{i}{\hbar}\bar{p}_r(x_r - \bar{x}_r), \quad (52)$$

$$\theta_1 = \begin{pmatrix} \frac{i}{\hbar} \mathcal{M}_{11}^l(x_l - \bar{x}_l) \\ -2\alpha\bar{x}'_l + 2\gamma\bar{x}'_r - \frac{i}{\hbar} p'_{i_1} + \frac{i}{\hbar} \mathcal{M}_{12}^l(x_l - \bar{x}_l) \\ \frac{i}{\hbar} \mathcal{M}_{11}^r(x_r - \bar{x}_r) \\ -2\alpha\bar{x}'_r + 2\gamma\bar{x}'_l - \frac{i}{\hbar} p'_{i_3} + \frac{i}{\hbar} \mathcal{M}_{12}^r(x_r - \bar{x}_r) \end{pmatrix}, \quad (53)$$

$$\hat{\theta}_2 = \begin{pmatrix} \beta_1 + \frac{i}{2\hbar} \mathcal{M}_{11}^l \mathcal{M}_{21}^l & \frac{i}{2\hbar} \mathcal{M}_{11}^l \mathcal{M}_{22}^l & 0 & 0 \\ \frac{i}{2\hbar} \mathcal{M}_{11}^l \mathcal{M}_{22}^l & \alpha + \frac{i}{2\hbar} \mathcal{M}_{12}^l \mathcal{M}_{22}^l & 0 & -\gamma \\ 0 & 0 & \beta_3 - \frac{i}{2\hbar} \mathcal{M}_{11}^r \mathcal{M}_{21}^r & -\frac{i}{2\hbar} \mathcal{M}_{11}^r \mathcal{M}_{22}^r \\ 0 & -\gamma & -\frac{i}{2\hbar} \mathcal{M}_{11}^r \mathcal{M}_{22}^r & \alpha - \frac{i}{2\hbar} \mathcal{M}_{12}^r \mathcal{M}_{22}^r \end{pmatrix}. \quad (54)$$

Most of the notation used is already obvious. From every "cell" or grid point depart two classical orbits with initial conditions $(p_{i_1}, \bar{x}'_l, p_{i_3}, \bar{x}'_r)$, where p_{i_1} and p_{i_3} vary along the 2D grid and the initial positions \bar{x}'_l and \bar{x}'_r are the average positions of the density matrix. After the classical propagation, the phase space location of the cell is $(\bar{p}_l, \bar{x}_l, \bar{p}_r, \bar{x}_r)$. Along the two classical orbits launched at each cell we also calculate the total stability matrices \mathcal{M}^l and \mathcal{M}^r .

The final formula for the generating function has thus been recast as a sum over two-orbit expansions (one per grid point). Each classical orbit in the chosen grid carries information about its immediate neighborhood. Having a set of orbits started on different points of the initial phase space allows one to describe nonlinear dynamics because the classical orbits are free to wander in phase space, each one following its own dynamics. This is in contrast with the two-orbit approximation used in a previous section, in which by expanding the actions and final position and momentum about the central guiding paths one restricted the dynamics to a limited region of phase space. The cellular implementation described here is numerically more expensive than the

simple two-orbit one because more orbits are required, but should allow the propagation of the dynamics for a very long time (high resolution in the spectra of eigenvalues).

Our description of the cellular implementation is the most general description for an arbitrary initial density matrix; in some cases it will be required to expand the dynamics in its full four-dimensional grid.

Finally if the initial density matrix is not Gaussian it is always possible to expand it as a sum over Gaussians and then apply the procedure outlined here to each element of the Gaussian basis.

VIII. CONCLUSIONS

In this work we have demonstrated that electronic coherent processes taking place in molecules under the influence of multiple short laser pulses do have a classical analog. The classical picture consists of a pair of classical orbits that guide the time evolution of the density matrix and that at appropriate times switch potential surfaces. The principal application made here is the description of nonlinear optical responses in terms of classical orbits for general systems.

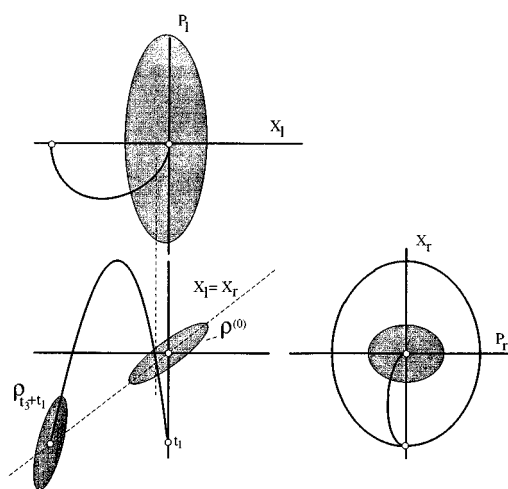


FIG. 16. Type B recurrence.

However, there are formal similarities between the problem presented here and the curve-crossing mechanism of inelastic scattering first addressed by Landau–Zener during the early 1930's.²⁶ They were concerned with the semiclassical estimate for the inelastic curve crossing in scattering processes. The Landau–Zener formula can be connected to our linear response function. Therefore it is possible to develop ways to improve on the Landau–Zener expression by using higher order nonlinear response functions.¹⁶

Because our approach is carried out directly in the time domain, the semiclassical mechanism for switching between electronic states is well defined. The time-domain formalism and the perturbation expansion allows a simple yet rigorous description of the surface crossing mechanism. Moreover, the generation of a single semiclassical propagator for the chain of Van Vleck operators provides a powerful tool for evaluating the complex time evolution operators of the generating functions. The use of semiclassical tools in the theory of nonlinear optical response appears to be very powerful. Thanks to the classical orbits it is possible to visualize and understand in its full four-dimensional phase space the dynamics of the density matrix and the effect of the field interactions on the motions of the molecular system.

The formalism presented does not contemplate dissipation. A future expansion of the current work would be to include some of the recent advances in the microscopic description of dissipation into our semiclassical dynamics. The incorporation of dissipation in the nonlinear response is important for the interpretation of condensed phase spectra. For harmonic systems, exactly solvable models for the time evolution of an electronic coherence with dissipation based on the spin Boson Hamiltonian have been used.^{18,27–29} It is possible to derive reduced equations of motion such as the nonlinear Fokker–Planck equation for anharmonic systems. Grossmann³⁰ had recently implemented the “cellular dynamics” method for a nonlinear molecular system coupled to a harmonic bath. The dissipation mechanism follows the Caldeira–Leggett²⁷ formalism and applies for single potential surface. Application of the semiclassical formalism presented

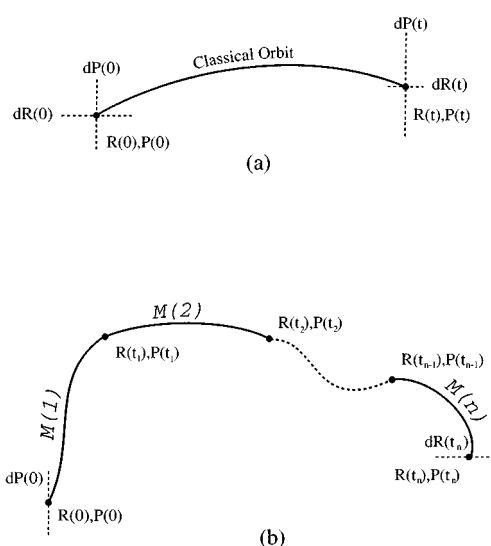


FIG. 17. Initial and final variations along (a) single orbit, and (b) multiply connected classical orbit for the semiclassical Liouville propagator.

here to the dissipative case seems promising.

ACKNOWLEDGMENTS

The support of the National Science Foundation and the Air Force Office of Scientific Research is gratefully acknowledged.

APPENDIX A: STABILITY ANALYSIS

Few notions from classical Hamiltonian mechanics are crucial to understand semiclassics. We start with Hamilton's equations of motion associated with the Hamiltonian H_1 :

$$\begin{aligned}\dot{P} &= -\frac{\partial H_1}{\partial R}, \\ \dot{R} &= \frac{\partial H_1}{\partial P}.\end{aligned}\quad (\text{A1})$$

A set of initial conditions, $P(0), R(0)$, specifies a unique classical trajectory via the time derivatives [Eq. (A1)], if a solution of the differential equations for that particular initial value exists. The behavior of the solution with respect to small variations of the initial conditions defines the stability of the classical orbit. Linearization of Hamilton's equations about the known solution determines the *monodromy* or *stability matrix*:

$$\begin{pmatrix} dP(t) \\ dR(t) \end{pmatrix} = M \begin{pmatrix} dP(0) \\ dR(0) \end{pmatrix}.\quad (\text{A2})$$

The time derivatives for the elements of matrix M_{ij} are obtained from Eqs. (A1) as

$$\dot{M} = \begin{pmatrix} (\partial^2 H_1 / \partial P^2) & (\partial^2 H_1 / \partial P \partial R) \\ (\partial^2 H_1 / \partial P \partial R) & (\partial^2 H_1 / \partial R^2) \end{pmatrix} M.\quad (\text{A3})$$

Figure 17(a) shows a classical orbit and illustrates the meaning of the variables dR, dP . Obviously the stability

equations [Eqs. (A3)] must be integrated numerically together with the equations of motion [Eq. (A1)].

The stability matrix M is very useful because it contains all the information required to calculate the semiclassical propagation. For example, the usual Van Vleck propagator $\langle R(0)|R(t)\rangle$ goes asymptotically as the square of the classical probability to go from $R(0)$ to $R(t)$ times a phase. Since the initial position is specified and only the initial momentum is unknown then this probability can be determined as the ratio $dP(0)/dR(t)$ keeping $dR(0)$ constant. In other words, $\langle R(0)|R(t)\rangle \sim |M_{21}|^{-1/2}$.

Now let us imagine a classical path that follows a sequential set of propagations [Fig. 17(b)]: the orbit starts at $R(0), P(0)$ and evolves under Hamiltonian H_1 for time t_1 , then it continues under a different Hamiltonian, H_2 , for time t_2 , etc., up to the n th step when $R(t_{n-1}), P(t_{n-1})$ is finally mapped onto $R(t_n), P(t_n)$ by the equations of motion of H_n . This unusual classical path is the one required for the calculation of the elements of matrix $\langle R(0)|\mathcal{Z}_i^j|R(t_n)\rangle$, Eqs. (19). This quantity also goes asymptotically as the square root of a classical probability, the probability of ending up somewhere around $R(t_n)$ when the classical orbit started around $R(0)$. Since the initial position is well specified we can calculate the probability as the ratio $dP(0)/dR(t)$. Now this ratio needs to be calculated differently than before because the time evolution from initial to final position has followed several different sets of equations of motion.

Let us define the stability matrices $M^{(i)}$ associated with each of the classical segments of the full path connecting $R(0)$ and $R(t_n)$. Then

$$\begin{pmatrix} dP(t_i) \\ dR(t_i) \end{pmatrix} = M^{(i)} \begin{pmatrix} dP(t_{i-1}) \\ dR(t_{i-1}) \end{pmatrix}. \quad (\text{A4})$$

Each of the matrices $M^{(i)}$ is calculated by solving the equations of motion of the stability matrix under Hamiltonian H_i .

The relationship between variations of the initial conditions $R(0), P(0)$ and the final point $R(t_n), P(t_n)$ along the classical path of interest can be easily expressed in terms of the stability matrix for the whole sequential process \mathcal{M} , easily shown to be

$$\mathcal{M} = M^{(n)} \cdot M^{(n-1)} \dots M^{(1)}. \quad (\text{A5})$$

Finally the matrix element of $\langle R_{t_n}|\hat{\mathcal{Z}}_i^j|R_0\rangle$ goes as $\sim |M_{21}|^{-1/2}$ when $\hbar \rightarrow 0$. The same applies for the right-hand side operator $|\hat{\mathcal{Z}}_i^j\rangle$.

Whether we consider the Van Vleck or the sequential propagator there is always the possibility of having several classical paths connecting initial and final conditions. In that case, the total amplitude will be a sum over the classical probabilities of each event.

In this Appendix we have focused on the classical probability part of the transition moment and not on its phase. As $\hbar \rightarrow 0$ on top of the $|M_{21}|^{-1/2}$ factor there is a phase given by the classical action accumulated along the orbit. This was discussed in Sec. VI.

APPENDIX B: COEFFICIENTS FOR THE TWO-PATH SEMICLASSICAL EXPANSION OF THE THIRD-ORDER RESPONSE

The coefficients used in Eq. (34) are defined as follows:

$$g = (2\hbar \mathcal{M}_{21}^l \alpha - i \mathcal{M}_{22}^l)(2\hbar \mathcal{M}_{21}^r \alpha + i \mathcal{M}_{22}^r) - 4\hbar^2 \mathcal{M}_{21}^r \mathcal{M}_{21}^l \gamma^2, \quad (\text{B1})$$

$$k_2 = \frac{i}{2\hbar} \left(\frac{\mathcal{M}_{11}^r}{\mathcal{M}_{21}^r} - \frac{\mathcal{M}_{11}^l}{\mathcal{M}_{21}^l} \right) - \frac{2\gamma}{g} + \frac{2\alpha \hbar \mathcal{M}_{21}^r + i \mathcal{M}_{22}^r}{2\hbar g \mathcal{M}_{21}^l} + \frac{2\alpha \hbar \mathcal{M}_{21}^l - i \mathcal{M}_{22}^l}{2\hbar g \mathcal{M}_{21}^r}, \quad (\text{B2})$$

$$k_1 = \frac{i}{\hbar} (\bar{p}_l - \bar{p}_r) - \frac{i \mathcal{M}_{11}^l}{\hbar \mathcal{M}_{21}^l} \bar{x}_l + \frac{i \mathcal{M}_{11}^r}{\hbar \mathcal{M}_{21}^r} \bar{x}_r + \frac{(2\alpha \hbar \mathcal{M}_{21}^r + i \mathcal{M}_{22}^r)}{g \hbar \mathcal{M}_{21}^l} \bar{x}_l + \frac{(2\alpha \hbar \mathcal{M}_{21}^l - i \mathcal{M}_{22}^l)}{g \hbar \mathcal{M}_{21}^r} \bar{x}_r - \frac{2\gamma}{g} (\bar{x}_l + \bar{x}_r), \quad (\text{B3})$$

$$k_0 = \frac{i}{\hbar} (\bar{S}_l - \bar{S}_r) + \frac{i}{\hbar} (\bar{x}_r \bar{p}_r - \bar{x}_l \bar{p}_l) + \frac{i \mathcal{M}_{11}^l}{2\hbar \mathcal{M}_{21}^l} \bar{x}_l^2 - \frac{i \mathcal{M}_{11}^r}{2\hbar \mathcal{M}_{21}^r} \bar{x}_r^2 + \frac{2\gamma \bar{x}_r \bar{x}_l}{g} - \frac{2\alpha \hbar \mathcal{M}_{21}^r + i \mathcal{M}_{22}^r}{2\hbar g \mathcal{M}_{21}^l} \bar{x}_l^2 - \frac{2\alpha \hbar \mathcal{M}_{21}^l - i \mathcal{M}_{22}^l}{2\hbar g \mathcal{M}_{21}^r} \bar{x}_r^2. \quad (\text{B4})$$

¹N. Bloembergen, *Nonlinear Optics* (Benjamin, New York 1965).

²S. Mukamel, *Principles of Nonlinear Optical Spectroscopy* (Oxford University, Oxford, 1995).

³*Ultrafast Phenomena IX*, edited by G. A. Mourou, A. H. Zewail, P. F. Barbara, and W. H. Knox (Springer, Berlin, 1994).

⁴E. T. J. Nibbering, P. A. Wiersma, and K. Duppen, *Phys. Rev. Lett.* **66**, 2464 (1991); **68**, 514 (1992).

⁵M. Orrit, J. Bernard, and R. I. Personov, *J. Phys. Chem.* **97**, 10 256 (1993); R. Jankowiak and G. J. Small, *Science* **237**, 618 (1987).

⁶P. Saalfrank, R. Baer, and R. Kosloff, *Chem. Phys. Lett.* **230**, 463 (1994).

⁷R. F. Loring and S. Mukamel, *Chem. Phys. Lett.* **114**, 426 (1985); *J. Opt. Soc. Am. B* **3**, 595 (1986).

⁸J. Cao and G. A. Voth, *J. Chem. Phys.* **99**, 10 070 (1993); **100**, 5093 (1994); **100**, 5106 (1994); G. Ilk and N. Makri, *ibid.* **101**, 6708 (1994); D. E. Makarov and N. Makri, *Chem. Phys. Lett.* **221**, 482 (1994).

⁹M. C. Gutzwiller, *Chaos in Classical and Quantum Mechanics*, Interdisciplinary Applied Mathematics (Springer, Berlin), Vol. 1.

¹⁰M. A. Sepulveda, S. Tomsovic, and E. J. Heller, *Phys. Rev. Lett.* **69**, 402 (1992); E. J. Heller, S. Tomsovic, and M. A. Sepulveda, *Chaos* **2**, 105 (1992).

¹¹P. W. O'Connor, S. Tomsovic, and E. J. Heller, *Physica D* **55**, 340 (1992); S. Tomsovic and E. J. Heller, *Phys. Rev. E* **47**, 282 (1992).

¹²J. H. Van Vleck, *Proc. Natl. Acad. Sci. U.S.A.* **14**, 178 (1928).

¹³M. C. Gutzwiller, *J. Math. Phys.* **8**, 1979 (1967); **10**, 1004 (1969).

¹⁴W. H. Miller, *Adv. Chem. Phys.* **25**, 69 (1974); *J. Chem. Phys.* **53**, 1949, 3578 (1970).

¹⁵S. Mukamel and Y. J. Yan, *Acc. Chem. Res.* **22**, 301 (1989).

¹⁶N. Makri, J. N. Gehlen, D. Chandler, and M. Newton, *J. Am. Chem. Soc.* **115**, 4178 (1993).

¹⁷L. E. Fried and S. Mukamel, *Adv. Chem. Phys.* **84**, 435 (1993).

- ¹⁸Y. Tanimura and S. Mukamel, Phys. Rev. A **46**, 118 (1992).
- ¹⁹R. G. Littlejohn, J. Stat. Phys. **68**, 7 (1992); J. B. Delos, Adv. Chem. Phys. **65**, 161 (1986).
- ²⁰M. A. Sepúlveda and E. J. Heller, J. Chem. Phys. **101**, 8004, 8016 (1994); K. Kay, *ibid.* **100**, 4432 (1994).
- ²¹E. J. Heller, Acc. Chem. Res. **14**, 368 (1981), and references therein.
- ²²E. J. Heller, J. Chem. Phys. **62**, 1544 (1975); **65**, 4979 (1976).
- ²³M. D. Feit and J. A. Fleck, J. Chem. Phys. **78**, 301 (1982).
- ²⁴E. J. Heller, J. Chem. Phys. **94**, 2723 (1991).
- ²⁵M. A. Sepúlveda, Ph. D. thesis, University of Washington, Seattle (1993).
- ²⁶C. Zener, Proc. R. Soc. London Ser. A **137**, 696 (1932); L. D. Landau and E. M. Lifshitz, *Mecánica Cuántica (Teoría No Relativista)* (Reverté, Barcelona, 1983), p. 374.
- ²⁷A. O. Caldeira and A. J. Leggett, Physica A **121**, 587 (1983).
- ²⁸H. Grabert, P. Schramm, and G. L. Ingold, Phys. Rep. **168**, 115 (1988).
- ²⁹M. Sparpaglione and S. Mukamel, J. Chem. Phys. **88**, 3263 (1988); Y. Hu and S. Mukamel, *ibid.* **91**, 6973 (1989).
- ³⁰F. Grossmann, J. Chem. Phys. (to be published).